https://doi.org/10.5194/cp-2020-63
Preprint. Discussion started: 12 May 2020

Climate of the Past Discussions

Sea Ice dynamics at the Western Antarctic Peninsula during the industrial era: a multi-proxy intercomparison study

Maria-Elena Vorrath[1], Juliane Müller[1,2,3], Lorena Rebolledo[4,5], Paola Cárdenas[4], Xiaoxu Shi[1], Oliver Esper[1], Thomas Opel[1], Walter Geibert[1], Práxedes Muñoz[6], Christian Haas[1], Carina B. Lange[4,7,8,9], Gerrit Lohmann[1], Gesine Mollenhauer[1,2]

[1]Alfred Wegener Institute, Helmholtz Centre for Polar and Marine Research, Bremerhaven, Germany

[2]MARUM – Center for Marine Environmental Sciences, University of Bremen, Germany

[3]Department of Geosciences, University of Bremen, Germany

[4]Centro de Investigación Dinámica de Ecosistemas Marinos de Altas Latitudes (IDEAL), Universidad Austral de Chile, Valdivia, Chile

[5]Instítuto Antártico Chileno (INACH), Punta Arenas, Chile

[6]Facultad de Ciencias del Mar, Universidad Católica del Norte, Coquimbo, Chile

[7]Centro Oceanográfico COPAS Sur-Austral, Universidad de Concepción, Chile

[8]Departamento de Oceanografía, Universidad de Concepción, Chile

[9]Scripps Institution of Oceanography, La Jolla, CA 92037, USA

Correspondence to: Maria-Elena Vorrath, maria-elena.vorrath@awi.de

Abstract. In the last decades, changing climate conditions have had a severe impact on sea ice at the Western Antarctic Peninsula (WAP), an area rapidly transforming under global warming. To study the development of spring sea ice and environmental conditions in the pre-satellite era we investigated three short marine sediment cores for their biomarker inventory with particular focus on the sea ice proxy $IPSO_{25}$ and micropaleontological proxies. The core sites in the Bransfield Strait are located in shelf to deep basin areas characterized by a complex oceanographic frontal system, coastal influence and sensitivity to large-scale atmospheric circulation patterns. We analyzed geochemical bulk parameters, biomarkers (highly branched isoprenoids, glycerol dialkyl glycerol tetraethers, sterols), and diatom abundances and diversity over the past 200 years (^{210}Pb dating), and compared them to observational data, sedimentary and ice core climate archives as well as results from numerical models. Based on biomarkers we could identify four different stratigraphic units with (1) stable conditions and moderate sea ice cover before 1860, (2) low to moderate sea ice cover between 1860 and 1930, (3) high seasonal variability

https://doi.org/10.5194/cp-2020-63
Preprint. Discussion started: 12 May 2020

Climate of the Past Discussions
Open Access
EGU

and changes in sea ice regimes from 1930 to 1990 and (4) a shift to increasing sea ice cover despite anthropogenic warming since 1990. Although $IPSO_{25}$ concentrations correspond quite well with satellite sea ice observations for the past 40 years, we note discrepancies between the biomarker-based sea ice estimates and the long-term model output for the past 200 years, ice core records and reconstructed atmospheric circulation patterns such as El Niño Southern Oscillation (ENSO) and Southern Annular Mode (SAM). We propose that the sea ice biomarker proxies $IPSO_{25}$ and $PIPSO_{25}$ are not linearly related to sea ice cover and, additionally, each core site reflects specific, local environmental conditions. High $IPSO_{25}$ and $PIPSO_{25}$ values may not be directly interpreted as referring to high spring sea ice cover because variable sea ice conditions and enhanced nutrient supply may affect the production of both the sea-ice associated and phytoplankton-derived (open marine, pelagic) biomarker lipids. For a more meaningful interpretation we recommend to carefully consider individually biomarker records to distinguish between cold, sea ice favoring and warm, sea ice diminishing environmental conditions.

Key Words: paleoclimate, Antarctic sea ice, highly branched isoprenoids, $IPSO_{25}$, diatoms, ENSO, SAM

1 Introduction

Observations of global mean surface temperatures show a warming since the industrialization of approximately 1.0±0.2°C (IPCC, 2018) above the 1850-1900 baseline. An acceleration of this trend due to anthropogenic forcing has been projected (IPCC, 2019). The ocean, and especially the Southern Ocean, takes up the majority of the atmospheric heat, and warming has already been observed at all depths (IPCC, 2019). Antarctica´s hot spot of warming is the Western Antarctic Peninsula (WAP) (Jones et al., 2016) with atmospheric temperature increases of 3.7±1.6°C per century (Vaughan et al., 2003) and a slight cooling from 2000 to 2010 (Turner et al., 2019). A warming of up to 1°C of subsurface water is evident in different water masses around the WAP (Cook et al., 2016). On land, glaciers and ice shelves on both sides of the Antarctic Peninsula (AP) retreat rapidly (Cook et al., 2016; Rignot et al., 2019), pointing towards a potential collapse of the WAP ice shelves. In the ocean, the loss of sea ice cover is significant (Parkinson and Cavalieri, 2012). Shortened sea ice seasons (Parkinson, 2002) and a reduction of sea ice extent accelerating from 4 % up to 10 % per decade (Liu et al., 2004) have been observed via satellite since 1979. A recent compilation shows that the slight increase in sea ice around the entire Antarctic continent since 1979 seems to be interrupted since 2014 (Parkinson, 2019). However, the region of the WAP, the Bellingshausen Sea and Amundsen Sea show contrasting sea ice trends and high sea ice variability in 2014 and afterwards (Hobbs et al., 2016). The changes in sea ice cover are not only related to warm water intrusion and higher sea surface temperatures (SSTs) at the WAP (Martinson and McKee, 2012; Meredith and King, 2005), but also to large-scale modes of atmospheric circulation such as the Southern Annular Mode (SAM) (e.g. Barbara et

https://doi.org/10.5194/cp-2020-63
Preprint. Discussion started: 12 May 2020


Climate of the Past Discussions
Open Access
EGU

al., 2013) and the El Niño Southern Oscillation (ENSO) (e.g. Liu et al., 2004), or a combination of both (Etourneau et al., 2013; Stammerjohn et al., 2008b, 2008a).

Sea ice is an important factor that shapes and influences the Southern Ocean. Melting sea ice releases nutrients and leads to enhanced primary production and ocean stratification during spring and summer (Arrigo et al., 1997; Vernet et al., 2008). Interestingly, a higher number of sea ice days is associated with to an increased photosynthetic efficiency and enhanced carbon fixation rates due to enhanced nutrient delivery stimulating primary production (Schofield et al., 2018) but also thinning of sea ice affects marine productivity positively (Hancke et al., 2018). Release of dense brine during sea ice formation influences the thermohaline circulation by feeding of deep and intermediate waters (Nicholls et al., 2009) but also induce upwelling at sea ice edges (Alexander and Niebauer, 1981). Sea ice cover also regulates the ocean-atmosphere exchange of heat and gases as well as regional precipitation and albedo (Allison et al., 1982; Butterworth and Miller, 2016; Turner et al., 2017) and is a potential source of the radiative-relevant volatile dimethylsulphide (Trevena and Jones, 2006) – a precursor of methanesulphonic acid (MSA) (Abram et al., 2010). Sea ice changes at the WAP may lead to the destabilization and/or collapse of local ice shelves due to warm water intrusions and basal melting (Cook et al., 2016; Etourneau et al., 2019; Hellmer et al., 2012) promoting an accelerated ice-sheet flow towards the ocean (Huss and Farinotti, 2014). Sea ice decline in this region may thus also indirectly impact global sea level rise.

Atmospheric circulation patterns such as ENSO and SAM have been suggested to influence the distribution of SST and sea ice at the WAP (Ding et al., 2012; Stammerjohn et al., 2008b, 2008a). Etourneau et al. (2013) concluded from the occurrence of higher sea ice cover together with higher SSTs that a rising number of ENSO events would increase the seasonal amplitude of warmer summers and colder winters in the region. SAM is the leading mode in the Southern Hemisphere (Jones et al., 2016) and has significant impacts on temperatures at the northeast AP (Clem et al., 2016). Stammerjohn et al. (2008b) link ENSO and SAM related teleconnections to opposite sea ice trends in the Pacific and Atlantic sector of the Southern Ocean on decadal scales during the satellite era. The high-latitude responses and ice-atmosphere anomalies are strongest when a positive ENSO occurs "in-phase" with a negative SAM (+ENSO/-SAM) and the subtropical jet over the Pacific Ocean is strengthening whereas the polar frontal jet and the westerlies are weaker. In this state, a positive sea level pressure establishes a high-pressure cell in the Pacific Southern Ocean and warmer, moister conditions with less sea ice establish there. Meanwhile, the Weddell Sea and the WAP experience a cooling with an advance of sea ice. During the opposite state (-ENSO/+SAM) a stronger polar frontal jet establishes a low-pressure cell in the Bellingshausen Sea. In this case, increased, south-ward migrated westerlies transport heat towards the WAP and the Weddell Sea and sea ice cover is reduced under high atmospheric and sea surface temperatures (Marshall et al., 2006; Stammerjohn et al.,

https://doi.org/10.5194/cp-2020-63
Preprint. Discussion started: 12 May 2020

Climate of the Past Discussions
Open Access
EGU

2008b; Yuan, 2004). Clem et al. (2016) describe that the combined effect of in-phase ENSO and SAM is strongest in spring.

For modelling past and future Antarctic climate, its ice sheet stability, the thermohaline circulation or the impacts of sea ice loss for ecosystems, data of past sea ice cover are crucial but barely available (Bracegirdle et al., 2015, 2019). For the WAP, insights into climate and sea-ice dynamics during the industrial era are available from ice cores (stable isotopes and marine aerosols) but information from high resolution marine sediments and in particular sedimentary, geochemical or diatom-based sea ice proxies remain sparse (Thomas et al., 2019). Sinking marine particles carry environmental information from the sea surface to the ocean floor and, when buried in the sediments, the environmental history including sea ice can be deduced from these marine climate archives. For sea ice reconstructions, the use of sea ice-associated diatom species and biogeochemical parameters are common (Crosta et al., 1998; Esper and Gersonde, 2014a; Gersonde and Zielinski, 2000). Since diatom frustules may be affected by the dissolution of biogenic opal in the photic zone (Ragueneau et al., 2000), on the ocean floor (Leventer, 1998) and in the sediments (Burckle and Cooke, 1983; Esper and Gersonde, 2014b), an increasing attention is directed to their molecular remains, i.e. specific biomarker lipids, as promising tools for past sea ice reconstructions (Massé et al., 2011). A specific diunsaturated highly branched isoprenoid alkene (HBI diene, $C_{25:2}$) has been proposed as potential tool for past spring sea ice reconstructions in the Southern Ocean (Massé et al., 2011). It is produced by sea ice diatoms (Nichols et al., 1988) and its sea ice origin is evident from the high $\delta^{13}C$ isotopic signature of the molecule (Massé et al., 2011; Sinninghe Damsté et al., 2007; Vorrath et al., 2019). The sea ice diatom *Berkeleya adeliensis* which is found in Antarctic landfast ice and platelet ice (Riaux-Gobin and Poulin, 2004) was identified as a producer of the HBI diene (Belt et al., 2016). HBI diene is present in surface and downcore sediments around Antarctica and can be used as $IPSO_{25}$ (**I**ce **P**roxy for the **S**outhern **O**cean with **25** carbon atoms) in analogy to the Arctic IP_{25} (Belt et al., 2016; Lamping et al., 2020; Massé et al., 2011; Vorrath et al., 2019). To differentiate among an extended spring sea ice cover, the occurrence of a stable sea ice margin and/or an open marine environment, $IPSO_{25}$ is combined with phytoplankton-derived biomarker from lipids such as HBI trienes and/or sterols, which are assumed to refer to open water conditions (Belt and Müller, 2013; Volkman, 1986). Analogous to the PIP_{25} index (P stands for open marine phytoplankton marker) for semi-quantitative sea ice estimations in the Arctic (Müller et al., 2011), the recently proposed $PIPSO_{25}$ approach (Vorrath et al., 2019) allows for a differentiation between several sea ice conditions of a permanently open ocean, a sea ice marginal zone and a permanent sea ice cover (Müller et al., 2011).

Here, we provide the first $IPSO_{25}$-based high-resolution assessment of the spring sea ice development at the WAP during the industrial era and examine the response of sea ice to changes in atmospheric and oceanic oscillation

https://doi.org/10.5194/cp-2020-63
Preprint. Discussion started: 12 May 2020


Climate of the Past Discussions

patterns. To achieve this, we conducted a multiproxy study on three short sediment cores from different depths and oceanic regimes within the Bransfield Strait. In addition to $IPSO_{25}$, we analyzed HBI trienes, sterols and glycerol dialkyl glycerol tetraethers (GDGTs) for subsurface ocean temperature (SOT) reconstruction as well as diatom assemblages for estimating winter sea ice concentrations (WSI) and summer sea surface temperatures (SSST) by means of transfer functions. We furthermore consider sea ice and temperature data from an atmosphere-sea ice-ocean numerical model (AWI-ESM2), historical surface air temperatures from local meteorological stations, ice core records (stable isotopes $\delta^{18}O$ and δD, MSA), and paleo records of atmospheric circulation patterns such as ENSO and SAM.

2 Material and Methods

2.1 Study Area

The study area is the Bransfield Strait at the northern tip of the WAP (Fig. 1a and b). The region includes the shallow shelf of the WAP as well as the Bransfield Basin with depths exceeding 2000 m at its deepest parts. The Bransfield Basin is located between the South Shetland Islands (SSI) to the northwest and the AP to the southeast. The shallow ocean has been shaped by ice sheet dynamics during the last glaciation (Canals and Amblas, 2016b; Ingólfsson et al., 2003) and several troughs discharge sediment load from the AP into the basin (Canals et al., 2016; Canals and Amblas, 2016a). The oceanographic setting in this area is complex and yet not fully constrained (Moffat and Meredith, 2018; Sangrà et al., 2011) because water masses enter the basin from the west and east (Fig. 1b). From the east, relatively cold (< 0°C) and salty Weddell Sea Water (WSW) flows at the surface alongshore the Antarctic mainland as a coastal current but also fills the Bransfield Basin completely below 150 m. It is also observed on the northern slope of the SSI at 200-600 m depth and around Elephant Island as a result of wind driven modulation (Meijers et al., 2016). The main source from the west is the Bellingshausen Sea Water (BSW), a branch of the Antarctic Circumpolar Current (ACC). This well-stratified, fresh and warm surface water flows along the slope of the SSI and forms the Peninsula Front with the WSW in the central Bransfield Strait, trending southwest-northeast parallel to the Antarctic mainland (Sangrà et al., 2011). Additionally, Circumpolar Deep Water (CDW) enters from the southwest as a subsurface current, forming the Bransfield Front to the BSW at 200m to 550m depth along the SSI slope (Sangrà et al., 2017). Both BSW and CDW are observed to turn and flow back at the northern side of the SSI (Sangrà et al., 2011). The mixing and transformation of the three water masses in the Bransfield Strait is yet not well understood but a study of iceberg drifts from Collares et al. (2018) showed that water from the Weddell Sea join waters from the Bellingshausen Sea in the vicinity of Trinity Island (Fig. 1b). It has been suggested that eddies between the Peninsula Front and the Bransfield Front are a key mechanism for water

https://doi.org/10.5194/cp-2020-63
Preprint. Discussion started: 12 May 2020


Climate of the Past Discussions
Open Access
EGU

exchange and/or upwelling (Sangrà et al., 2011; Zhou et al., 2002) and meltwater discharge from the adjacent glaciers has to be considered (Meredith et al., 2018). In the southwest, south of the Bransfield Strait, a narrow, fast flowing Antarctic Peninsula Coastal Current (APCC) is present, enriched in glacial freshwater and characterized by downwelling (Moffat and Meredith, 2018).

Primary productivity at the WAP is mainly controlled by eddies and fronts (Gonçalves-Araujo et al., 2015), due to upwelling (Sangrà et al., 2011), sea ice dynamics (Vernet et al., 2008) and iron distribution (Klunder et al., 2014). High productivity regimes and high chlorophyll concentrations are found north of the Peninsula Front along the SSI under the influence of the BSW, while the area influenced by the WSW is characterized by lower production of nanoplankton (Gonçalves-Araujo et al., 2015). Upwelling, iron fertilization and sea-ice retreat lead to high interannual variability in the production patterns and a strong onshore-offshore gradient is evident. In consequence high production is related to coastal areas, shallow mixed layers and higher stratification owing to sea ice melting (Sanchez et al., 2019; Vernet et al., 2008). High production is also reflected in high vertical export of sinking particles (e.g. Wefer et al., 1988; Kim et al., 2004) and in the biogeochemical distribution of surface sediments, dominated by high concentrations of TOC, pigments, sterols and diatoms but low calcium carbonate (Cárdenas et al., 2019). Organic matter is mainly of marine origin as supported by low values of C/N and the stable carbon isotope composition (Cárdenas et al., 2019) whereas the AP is an important source of terrestrial silt and clay input (Wu et al., 2019).

2.2 Sampling and age model

The cores were collected in 2016 during the RV *Polarstern* cruise PS97 (ANT-XXXI/3) using multicorers at stations PS97/056-1 (63°45.42'S, 60°26.51'W, 633 m water depth) east of Trinity Island, PS97/068-2 (63°10.05'S, 59°18.12'W, 794 m water depth) in the Orleans Trough, and PS97/072-2 (62°00.39'S, 56°03.88'W, 1992 m water depth) in the East Bransfield Basin (Fig. 1b). Smear slides were examined and microscopic description of the surface sediments was done onboard (Lamy, 2016). Immediately after recovery of the sediments were sectioned in 1 cm slices and samples designated for biomarker analyses were stored frozen in glass vials, while separate samples for micropaleontological investigation were stored at 4° C in plastic bags. A second suite of samples from a trigger core from station PS97/072-1 was used for total organic carbon (TOC) and diatom analyses (diatom samples from core PS97/072-2 were not available).

Geochronology for the sediment cores from sites PS97/056-1 and PS97/072-2 was established using $^{210}Pb_{xs}$ activities quantified by alpha spectrometry of its daughter ^{210}Po in secular equilibrium with ^{210}Pb and using ^{209}Po as a yield tracer (Flynn, 1968). The activities were corrected to the time of plating considering the ^{210}Po decay (half life: 138 days). $^{210}Pb_{xs}$ (unsupported) activities were determined as the difference between ^{210}Pb and ^{226}Ra

https://doi.org/10.5194/cp-2020-63
Preprint. Discussion started: 12 May 2020

activities measured by gamma spectrometry in some intervals of the sediment core. Alpha and gamma counting were performed at the Laboratoire Géosciences of the Université de Montpellier (France). The ages were based on $^{210}Pb_{xs}$ inventories according the Constant Rate of Supply Model (CRS, Appleby and Oldfield, 1978). Standard deviations (SD) were estimated propagating the counting uncertainties (Bevington et al., 1993). Since the dating on core PS97/056-1 and PS97/072-2 was done on selected samples the age model was established using the software R (R Core Team, 2017) and the package clam (Blaauw, 2010, version 2.3.2, calibration curve Marine13.14C). Trigger core PS97/072-1 was correlated to the age model of core PS97/072-2 based on TOC data. $^{210}Pb_{xs}$ for core PS97/068-2 was measured at the Alfred Wegener Institute (AWI, Germany) on dried and ground bulk sediment samples in sealed gas-tight petri dishes, using a HPGe gamma spectrometer with planar geometry. ^{210}Pb was measured at 46 keV, ^{226}Ra for the excess correction in each depth interval via its indirect decay products at 295, 352 and 609 keV. Analytical errors were calculated considering error propagation. For core PS97/068-2 the calculation of CRS ages and the Monte-Carlo approximation of age uncertainties was based on Sanchez-Cabeza et al. (2014), modified to accommodate the variable sample sizes and fractions for different depths. Due to residual inventory of $^{210}Pb_{xs}$ below the available samples in cores PS97/056-1 and PS97/072-2, the CRS model had increasing uncertainties below ~130 years (supplement S1). We therefore extrapolated ages before 1880 based on the average respective sedimentation rates for the oldest 3 cm.

2.3 Organic geochemical analyses

Organic geochemical analyses were done on freeze-dried and homogenized sediments. Bulk content of carbon (C) and nitrogen (N) were determined with a CNS analyzer (Elementar Vario EL III, standard error < 2%), whereas the analysis of TOC content was done on 0.1 g acidified (500 µl hydrochloric acid) sediment using a carbon-sulphur determinator (CS-2000, ELTRA, standard error < 0.6 %). The C/N ratio was calculated as TOC/total nitrogen.

The extraction procedure of HBIs follows the analytical protocol of the international community conducting HBI-based sea ice reconstructions (Belt et al., 2013, 2014; Stein et al., 2012). For the quantification of biomarkers the internal standards 7-hexylnonadecane (7-HND), 5α-androstan-3β-ol and C_{46} were added to the sediments. Sediment samples of 5 g were extracted ultrasonically three times using 6 ml of CH_2Cl_2:MeOH (v/v 2:1, 15 min) followed by centrifugation (2500 rpm, 1 min) and decantation of the total organic solvent extract. The different biomarkers were separated via open column chromatography with silica gel used as a stationary phase. First, the apolar fraction containing HBIs was separated with 5 ml hexane, while the second polar fraction containing GDGTs and sterols was eluted with 5 ml CH_2Cl_2:MeOH (v/v 1:1). The polar fraction (GDGT and sterols) was dried using nitrogen, re-dissolved in 120 µl hexane:isopropanol (v/v 99:1) and filtered through a

https://doi.org/10.5194/cp-2020-63
Preprint. Discussion started: 12 May 2020


Climate of the Past Discussions

polytetrafluoroethylene filter (0.45 µm in diameter). After measuring GDGTs, the polar fraction was silylated (200 µl BSTFA; 60° C; 2 hours) and used for sterol analysis.

The HBIs and sterols were analyzed by GC-MS with an Agilent 7890B gas chromatograph equipped with a 30 m DB 1 MS column (0.25 mm diameter, 0.250 µm film thickness) and coupled to an Agilent 5977B mass spectrometer (MSD, 70 eV constant ionization potential, ion source temperature 230° C). Apolar and polar lipid fractions were analyzed using different temperature programs. For HBIs, the temperature was held at 60° C for 3 min, ramped to 325° C over 23 min, and was held at this level for 16min. Sterol analysis started at a temperature of 60° C for 2 min, followed by a temperature increase to 150° C over 6 min, and to 325° C within 57 min. HBIs were identified via comparison of mass spectra of the measured compounds and published mass spectra (Belt et al., 2000). Quantification of HBIs was based on manual peak integration. Instrumental response factors of molecular ions of HBI diene (*m/z* 348) und trienes (*m/z* 346) were determined by means of calibration measurements using a sample with known concentrations of HBIs. Identification of sterols was based on comparison of their retention times and mass spectra with those of reference compounds analyzed on the same instrument. The mean relative error of duplicates was < 5% for HBIs and < 1% for sterols (desmosterol had exceptional high relative errors of up to 14%), the detection limit was determined at 0.5 ng/g sediment. Co-elution of other compounds hampered identification and quantification of sterols in several samples (PS97/056-1; 0-13cm and PS97/072-2; 0-16cm).

GDGTs were analyzed using high performance liquid chromatography (HPLC, Agilent 1200 series HPLC system) coupled to a single quadrupole mass spectrometer (MS, Agilent 6120 MSD) via an atmospheric pressure chemical ionization (APCI) interface. Individual GDGTs were separated at 30° C on a Prevail Cyano column (150 mm x 2.1 mm, 3 µm). Each sample was injected (20 µl) and passed a 5 min isocratic elution with mobile phase A (hexane/2-propanol/chloroform; 98:1:1) at a flow rate of 0.2 ml/min. The mobile phase B (hexane/2-propanol/chloroform; 89:10:1) increased linearly to 10% within 20 min and after this to 100% within 10 min. After 7 min the column was cleaned with a backflush (5 min, flow 0.6 ml/min) and re-equilibrated with solvent A (10 min, flow 0.2 ml/min). The APCI had the following conditions: nebulizer pressure 50 psi, vaporizer temperature 350°C, N_2 drying gas temperature 350°C, flow 5 l/min, capillary voltage 4 kV, and corona current 5 µA. GDGT detection was done by selective ion monitoring (SIM) of $(M+H)^+$ ions (dwell time 76ms). The molecular ions *m/z* of GDGTs-I (*m/z* 1300), GDGTs-II (*m/z* 1298), GDGTs-III (*m/z* 1296), and Crenarchaeol (*m/z* 1292) as well as of the branched GDGTs-Ia (*m/z* 1022), GDGTs-IIa (*m/z* 1036), GDGTs-IIIa (*m/z* 1050) and hydroxylated GDGTs OH-GDGT-0 (*m/z* 1318), OH-GDGT-1 (*m/z* 1316), and OH-GDGT-2 (*m/z* 1314) were quantified in relation to

https://doi.org/10.5194/cp-2020-63
Preprint. Discussion started: 12 May 2020


Climate of the Past Discussions
Open Access
EGU

the internal standard C_{46} (*m/z* 744). The hydroxylated GDGTs were quantified in the scans of their related GDGTs (see Fietz et al., 2013). The standard deviation was 0.01 units of TEX^{L}_{86}.

We follow Kalanetra et al. (2009), proposing that GDGT-derived temperatures represent near-surface waters which is underlined by studies from Kim et al. (2012) and Park et al. (2019) and consider our results to reflect subsurface ocean temperatures (SOT). For calculation of TEX^{L}_{86} (Kim et al., 2010) only GDGTs with the *m/z* 1296 (GDGT-3), *m/z* 1298 (GDGT-2), *m/z* 1300 (GDGT-1) were considered in Eq. (1):

$$TEX^{L}_{86} = \log\left(\frac{[GDGT-2]}{[GDGT-1]+[GDGT-2]+[GDGT-3]}\right) \quad (1)$$

and calibrated it with Eq. (2) $SOT^{TEX} = 67.5 \times TEX^{L}_{86} + 46.9$ (Kim et al., 2010). (2)

The calculation based on OH-GDGT was done after Lü et al. (2015) in Eq. (3)

$$RI-OH' = \frac{[OH-GDGT-1]+2\times[OH-GDGT-2]}{[OH-GDGT-0]+[OH-GDGT-1]+[OH-GDGT-2]} \quad (3)$$

and calibrated with Eq. (4) $SOT^{OH} = (RI\text{-}OH' - 0.1) / 0.0382$. (4)

To determine the influence of terrestrial organic matter the BIT index was calculated following Hopmanns et al. (2004) as Eq. (5)

$$BIT = \frac{[GDGT-Ia]+[GDGT-IIa]+[GDGT-IIIa]}{[Crenarchaeol]+[GDGT-Ia]+[GDGT-IIa]+[GDGT-IIIa]}. \quad (5)$$

The phytoplankton-$IPSO_{25}$ index ($PIPSO_{25}$) was calculated following Eq. (6) from Vorrath et al. (2019) with

$$PIPSO_{25} = \frac{IPSO_{25}}{IPSO_{25}+(c\times phytoplankton\ marker)} \quad (6)$$

using sterols and HBI trienes as phytoplankton marker (Vorrath et al., 2019). The balance factor c (c = mean $IPSO_{25}$ / mean phytoplankton biomarker) is used to account for concentration offsets between $IPSO_{25}$ and phytoplankton biomarkers (Belt and Müller, 2013; Müller et al., 2011; Smik et al., 2016b; Vorrath et al., 2019). Since the concentrations of HBI trienes are within the same range as the sea ice proxy we set the c-factor to 1 (Smik et al., 2016b) and c-factors for sterols were calculated individually for every core site (supplement Table 1). To distinguish the different indices based on their phytoplankton marker we use the terms P_ZIPSO_{25} for an index based on Z-trienes, P_EIPSO_{25} based on E-trienes, P_BIPSO_{25} based on bassicasterol, and P_DIPSO_{25} based on dinosterol.

2.4 Diatom analysis and transfer functions

Diatom analyses were done on cores PS97/056-1, PS97/068-2 and the trigger core from the core site of PS97/072-1 (correlated with PS97/072-2 via TOC content). About 300 mg of freeze-dried sediments were treated after the method described by Cárdenas et al. (2019) to prepare slides for microscopy analysis. Two permanent slides per sample were prepared and observed with a Carl Zeiss Axio Lab.1 microscope with phase contrast at 1000× magnification at the Instituto Antártico Chileno in Punta Arenas. Diatoms were identified and counted on transects

https://doi.org/10.5194/cp-2020-63
Preprint. Discussion started: 12 May 2020


Climate of the Past Discussions
Open Access
EGU

on microslides until reaching at least 400 valves on each slide, following counting procedures of Schrader and Gersonde (1978). Diatom identification was done to species or species group level following the taxonomy described by Armand and Zielinski (2001), Taylor et al. (2001), Crosta et al. (2004), Buffen et al. (2007), Cefarelli et al. (2010), Esper et al. (2010), Allen (2014), and Campagne et al. (2016). The Hyalochaete of the genus *Chaetoceros* were identified as vegetative cells and/or resting spores.

We applied the marine diatom transfer function TF MAT-D274/28/4an to estimate winter sea ice (WSI) concentrations. It comprises 274 reference samples with 28 diatom taxa and/or taxonomic groups and an average of 4 analogues from surface sediments in the Atlantic, Pacific, and western Indian sectors of the Southern Ocean(Esper and Gersonde, 2014a). Winter sea ice (WSI) estimates reflect September sea-ice concentrations averaged over the period from 1981-2010 (National Oceanic and Atmospheric Administrations, NOAA; Reynolds et al., 2002, 2007) in a 1 by 1 grid. We follow the approach of Zwally et al. (2002) and define a sea ice concentration of 15% as the threshold for presence or absence of sea ice and 40% as the representative average of sea-ice edge (Gersonde et al., 2005; Gloersen et al., 1993). For summer sea surface temperature (SSST), we used the transfer function TF IKM336/29/3q from 336 reference samples (Pacific, Atlantic and Indian Southern Ocean) with 29 diatom taxa and three factors (Esper and Gersonde, 2014b). For calculations of MAT and IKM the software R (R Core Team, 2017) was used with the packages Vegan (Oksanen et al., 2012) and Analogue (Simpson and Oksanen, 2012).

2.5 Modelled data

We used data from numerical modelling to compare and evaluate our biogeochemical analyses. The AWI-ESM2 is a state-of-the-art coupled climate model developed at AWI (Sidorenko et al., 2019). The model consists of the atmospheric model ECHAM6 (Stevens et al., 2013) and the finite element sea ice-ocean model (FESOM2) (Danilov et al., 2017). The model also includes a Land-Surface Model (JSBACH) with dynamical vegetation (Raddatz et al., 2007).

The atmosphere grid in the high-resolution experiment is T63 (about 1.9 degree) with 47 vertical levels. A multi-resolution approach is employed in the ocean module. In detail, the high-resolution experiment applies up to 20 km horizontal resolution over the Arctic region and 150 km for the far field ocean (supplements S2). Moreover, the tropical belt has a refined resolution of 30-50 km in this configuration. There are 46 uneven vertical depths in the ocean component. The model has been validated under modern climate condition (Sidorenko et al., 2019). Previous versions of the model have been applied for the Holocene (Shi et al., 2020; Shi and Lohmann, 2016).

We run the climate model from the Mid-Holocene as a starting point (*midHolocene* simulation), and performed a transient simulation from the Mid-Holocene to the pre-industrial (*past6k* simulation) along the recipe as described

https://doi.org/10.5194/cp-2020-63
Preprint. Discussion started: 12 May 2020


Climate of the Past Discussions

in Otto-Bliesner et al. (2017). The transient orbital parameters are calculated according to Berger (1978). Moreover, as the change of topography from mid-Holocene to present is minor, we use constant topography under pre-industrial conditions for the entire transient period. In our modeling strategy, we follow Lorenz and Lohmann (2004) and use the climate condition from the pre-industrial state as spinup and initial state for the transient simulation covering the period 1850-2017 CE. Greenhouse gases concentrations are taken from the ice core records (Köhler et al., 2017) and from Meinshausen et al. (2011).

2.6 Additional data sets

Regional monthly satellite sea ice concentrations were derived from Nimbus-7 SMMR and DMSP SSM/I-SSMIS passive microwave data from the National Snow and Ice Data Center (NSIDC, grid cell size 25x25 km, Cavalieri et al., 1996) and mean winter (JJA) and spring (SON) sea ice concentrations were used in this study.

For the large-scale atmospheric modes we used the paleo ENSO index from Li et al. (2013) and the modelled SAM data from Abram et al. (2014). After Stammerjohn et al. (2008b), years with positive ENSO and negative SAM indices cause higher sea ice cover at the WAP and years with a negative ENSO and positive SAM lead to warmer seasons with reduced sea ice cover.

We used ice core stable isotope data representing relative air temperature at James Ross Island (δD, Abram et al., 2013) and at Bruce Plateau ($\delta^{18}O$, Goodwin et al., 2016). We compared the marine sea ice proxies (biomarkers, diatoms) with MSA data from coastal West Antarctic Dyer Plateau ice core (Abram et al., 2010).

3 Results

3.1 Age model and core description

The ^{210}Pb signals indicated continuously increasing ages with depth in all sediment cores (Fig. 2). All sediment cores roughly cover the last 240 years (including the extrapolated time) with resolution between 2 and 12 years per centimeter and sedimentation rates from 0.1 to 0.5 cm/a (supplementary Tables 2-4). Core PS97/056-1 located east of Trinity Island is characterized by silt-bearing diatomaceous clay (Lamy, 2016) and covers the timespan from 1830 to 2006 CE with sedimentation rates increasing from 0.1 to 0.4 cm/a over time. Core PS97/068-2 from Orleans Trough consists mainly of diatom-bearing silty clay (Lamy, 2016) and spans from 1780 to 2007 CE with sedimentation rates from 0.1 to 0.5 cm/a. Sediment core PS97/072-2 from the East Bransfield Basin is the deepest record characterized as silt-bearing diatomaceous clay (Lamy, 2016) with increasing sedimentation rates (from 0.1 to 0.4 cm/a) covering the time from 1823 to 2000 CE. The TOC contents of all cores ranged between 0.7 and 1.1 wt%. Low C/N ratios (< 8.6) and BIT values (< 0.02) point to a marine origin of the organic matter (supplementary Table 2-4).

https://doi.org/10.5194/cp-2020-63
Preprint. Discussion started: 12 May 2020


Climate of the Past Discussions

3.2 Biomarker lipids

A summary of biomarker results that will be discussed in detail is visualized in Figure 3 (results of HBI E-trienes, sterols and their related sea ice indices can be found in Figure S3 in the supplements, all data in supplementary Table 2-4). All biomarker records show an overall increasing trend towards the present with a few exceptional peaks along the record. $IPSO_{25}$ is abundant at all core sites with values ranging from 0.2 µg g^{-1} TOC up to 6.4 µg g^{-1} TOC. All three cores display similar patterns with low values before 1850 CE followed by moderate concentrations until 1970 CE and maxima in the 2000s (Fig. 3). Concentrations of HBI trienes are much lower than $IPSO_{25}$ concentrations with values below 1.4 µg g^{-1} TOC for Z-trienes (Fig. 3) and below 0.7 µg g^{-1} TOC for E-trienes (supplement S3). The exception is core PS97/072-2 from of the East Bransfield Basin where both HBI trienes reach up to 3.7 µg g^{-1} TOC and 1.6 µg g^{-1} TOC, respectively, in the second half of the 19th century. The concentrations of brassicasterol (10.2–241.3 µg g^{-1} TOC) and dinosterol (5.0–145.2 µg g^{-1} TOC) are two to three magnitudes higher than the HBIs; markedly lower concentrations characterize the Orleans Trough (PS97/068-2) (supplement S3). The $PIPSO_{25}$ indices calculated with Z- and E-trienes run parallel to $PIPSO_{25}$ based on brassicasterol and dinosterol and show increasing trends with time. In general, HBI triene-based $PIPSO_{25}$ have higher values (P_ZIPSO_{25} from 0.32 to 0.91; P_EIPSO_{25} from 0.25 to 0.95) than $PIPSO_{25}$ based on sterols (P_BIPSO_{25} from 0.15 to 0.70; P_DIPSO_{25} from 0.11 to 0.75). The $PIPSO_{25}$ indices suggest an increasing spring sea ice cover over time (Fig. 3, supplement S3). This is most prominent at the East Bransfield Basin (PS97/072-2) where lowest sea ice cover is indicated around 1870 CE and increase towards the present is indicated. Indications of short-term low spring sea ice cover are found for the 1960s and 1970s at the near-coastal core sites (PS97/056-1 and PS97/068-2) but do not change the overall trend.

Temperatures based on GDGTs show a wide range of values. At Trinity Island (PS97/056-1) and the East Bransfield Basin (PS97/072-2), SOT^{TEX} range from -3.87°C to 2.34°C (Fig. 3) whereas temperatures are always above zero from 0.73° C to 3.62° C at the Orleans Trough (PS97/068-2). Distinct cold events occur in the 1860s at the East Bransfield Basin (PS97/072-2) and as a longer cool period from 1940 to 1970 CE at the coastal core sites but general trends are hard to distinguish. In contrast, SOT^{OH} displays a decreasing temperature trend at all core sites with a narrow range of -2.58 °C to -0.99° C reversed by rapid warming since the 1990s (Fig. 3).

3.3 Diatom assemblages

Winter sea ice estimations derived from diatom assemblages point to a high variability (74% to 92% WSI at PS97/056-1, 64% to 92% at PS97/068-2, 68% to 90% at PS97/072-1) with a minimum around 1840 and 1880 CE and a slight increment toward 1990s (Fig. 3, supplementary Table 2, 3, 5). This variability coinciding with the high abundances of sea ice diatom species *Fragilariopsis curta* that show a high contribution at cores PS97/056-

https://doi.org/10.5194/cp-2020-63
Preprint. Discussion started: 12 May 2020


Climate of the Past Discussions

1 and 068-2 (supplement Tables 2 and 3). In addition, WSI records reveal similar features compared to $IPSO_{25}$ and $PIPSO_{25}$, which points to a relationship of winter and spring sea ice estimates based on different approaches. The SSST from diatom assemblages have a small amplitude in all cores (-0.9 to 0.5°C at PS97/056-1, -1.1 to 0.2°C at 068-2 and -0.8 to 0.1°C at 072-1) and show a similar pattern to SOT^{TEX} at the sites PS97/068-2 and 072-1 (Fig. 3, supplementary Table 2, 3, 5).

3.4 Modelled data

We use model data as derived from the AWI-ESM2 which include spring sea ice concentration (mSSIC), spring sea ice thickness (mSSIT), subsurface ocean temperature (mSOT, mean temperature from 30-100 m below sea surface), and surface air temperature (mSAT) (supplementary Table 6). Based on 10-year means, we detect negative trends for the last 200 years in both mSSIC (decrease by 30% to 50%) and mSSIT (decrease from 0.5 m down to 0.1 m). At the same time, positive trends for mSOT and mSAT at all core sites show temperatures rising by 0.3°C to 0.6°C. Further, a time series of the latitudinal shift of the sea ice edge at the WAP (between 50°W and 70°W) which shows a southward shift of 1.5° from 61.9°S to 63.4°S in the 20th century (supplementary Table 6).

4 Discussion

4.1 Spatial and temporal distribution of paleoenvironmental biomarkers

The core site at Trinity Island (PS97/056-1) is dominated by the APCC and receives freshwater input from the Peninsula with influence of BSW from the ACC (Moffat and Meredith, 2018). We suggest that sea ice proxies originate from free floating or land fast sea ice in this region since the core site is only 8 km away from Trinity Island. Coastal upwelling of macro- and micronutrients, especially iron, and a stratified water column fuel open marine primary production (Sanchez et al., 2019; Vernet et al., 2008) and may explain highest concentrations of sterols at this core site. $IPSO_{25}$, HBI Z-triene, P_ZIPSO_{25} and WSI records exhibit similar trends and fluctuations over time (Fig. 3). A direct relation between reconstructed sea ice conditions and temperature (SSST, SOT^{TEX} and SOT^{OH}) is not evident. However, slightly higher temperatures deduced from SOT^{OH} and diatom data seem to coincide with lower $IPSO_{25}$ concentrations, lower $PIPSO_{25}$ values and reduced WSI in the 19th century, while variable but higher temperatures in the 20th century are accompanied by higher IPSO25 and WSI concentrations at site PS97/056-1 (Fig. 3). The remarkably low SOT^{TEX} in the year 2006 CE might be a result of cold meltwater injections due to enhanced glacier melting (e.g. Pastra Glacier on Trinity Island). A general weak cooling trend is present in SSST and SOT^{OH} from 1920 CE to the 1990s.

The data obtained from the sediment core in the Orleans Trough (PS97/068-2) suggest that the core site is affected by the Peninsula Front where water masses from both salty and cold WSW and fresh and warm BSW meet. The

https://doi.org/10.5194/cp-2020-63
Preprint. Discussion started: 12 May 2020


Climate of the Past Discussions

water here is characterized by enhanced mixing within a narrow eddy zone and deepening of the mixed layer (Sangrà et al., 2011). High concentrations of biomarkers point towards a strengthening of primary productivity associated with BSW (Gonçalves-Araujo et al., 2015) in a less stratified and mixed water column (Vernet et al., 2008). The patterns of $IPSO_{25}$, HBI Z-triene as well as P_ZIPSO_{25} and WSI have a good visual correspondence. They indicate higher phytoplankton productivity and higher sea ice cover towards present time. Also, SSST corresponds quite well with SOT^{OH} at PS97/056-1 and with SOT^{TEX} at PS97/072-2 (Fig. 3). The SOT^{TEX} is remarkably high (above 0° C) throughout the studied period contrasting modern ocean temperatures of the upper 400 m at the WAP below -0.5°C (Cook et al., 2016). Compared to SOT^{TEX}, SOT^{OH} temperatures are closer to modern ocean temperatures in this area (Cook et al., 2016) within a narrow range. As this core site is in the middle of BSW and WSW influenced, no clear dominance from one or the other regime is evident and we suggest that GDGT-derived temperatures are affected by influences of both BWS and WSW.

The core site in the East Bransfield Basin (PS97/072-2) is further away from the coast (145 km) compared to the other two core sites. Marine productivity is expected to be lower due to the presence of WSW (Gonçalves-Araujo et al., 2015) but relatively high concentrations of $IPSO_{25}$ and HBI Z-triene may be related to fertilization through iron input (Sanchez et al., 2019). A remarkable maximum in HBI Z-triene concentrations in the late 19th century have resulted from drastic changes in the local oceanographic settings and productivity patterns. As indicated by SOT^{TEX}, this period is marked by a rapid shift from cold to warm water temperatures, pointing to a possible dominance of warmer BSW. A corresponding retreat of sea ice cover and likely ice-free summers, as reflected by P_ZIPSO_{25} and WSI values, could have promoted the productivity of open marine or coastal phytoplankton communities, e.g. *Rhizosolenia* and *Pleurosigma*, synthesizing the HBI Z-triene (Belt et al., 2000, 2017).

Despite the different oceanographic settings, all cores sites exhibit increasing trends in $IPSO_{25}$ and HBI Z-triene concentrations as well as rising P_ZIPSO_{25} values and WSI towards the present reflecting an overall advance of sea ice cover. At the same time, SOT^{TEX} and SOT^{OH} tend to decrease until the 1990s and rise since the 1990s, which we interpret as a delayed ocean warming compared to other parts of the global ocean (Cook et al., 2016). The overall trend in our records is a rise of both open marine and sea ice biomarkers and an ocean cooling (mainly indicated by SOT^{OH}). A clear stratigraphy is hard to distinguish but four units could be roughly divided by sea ice and temperature biomarker records:

Unit A: Moderate sea ice cover before 1850 CE. In the period before 1850 CE, the WAP experienced low productivity of sea ice algae as well as ice-edge or open marine algae (low $IPSO_{25}$ and HBI triene values). Diatom and biomarker sea ice indices reveal decreasing winter sea ice and moderate spring sea ice cover with low variability in seasonal sea ice changes. The fluctuating water temperatures display no clear trend

https://doi.org/10.5194/cp-2020-63
Preprint. Discussion started: 12 May 2020


Climate of the Past Discussions
Open Access
EGU

except for a weak cooling at the East Bransfield Basin, which may have resulted from an enhanced WSW inflow into the Bransfield Strait.

Unit B: Moderate winter sea ice cover and ice-free summers from 1850 to 1930 CE. In this period, changes in the oceanographic pattern may have led to a dominance of BSW in the East Bransfield Basin (PS97/072-2) and a weakened WSW inflow causing sea ice retreat and ocean warming. During this time, seasonal shifts from winter sea ice to ice-free summers occurred faster and promoted enhanced open marine biomarker production (Gonçalves-Araujo et al., 2015) fueled by high nutrient release through melting (Vernet et al., 2008). Sea ice cover remained at a moderate level near the coast (core sites PS97/056-1 and 068-2), as suggested by Barbara et al. (2013) who interpreted near-coastal diatom assemblages and HBIs at both sides of the AP to reflect long persisting sea ice cover in spring (supplement S4). They furthermore postulated that enhanced productivity occurs due to a stratified water column and nutrient injections by meltwater and autumn storm activity in the southern Bransfield Strait. Despite this, we see high fluctuations of winter sea ice (up to 20% WSI between two data points). Furthermore, high (low) winter sea ice cover as indicated by WSI at PS97/068-2 and 072-2 occurs contrary to low (high) spring sea ice reflected by $P_Z IPSO_{25}$ pointing to fast seasonal changes.

Unit C: Higher variability and increasing sea ice cover from 1930 to 1990 CE. In contrast to Unit B, all biomarkers indicate an increasing sea ice cover in Unit C. It is characterized by a general ocean cooling (except for SSST in the East Bransfield Basin), which may suggest a delayed onset of anthropogenic warming in Antarctic waters (Abram et al., 2016; Cook et al., 2016) and the atmosphere (Abram et al., 2013). High fluctuations in $IPSO_{25}$ and HBI Z-triene concentrations indicate conditions favorable for both sea ice and phytoplankton productivity potentially resulting from a higher seasonal variability characterized by high winter sea ice cover and ice-free summers. High winter sea ice cover now coincides with high spring sea ice coverat all core sites. WSI and $IPSO_{25}$ indicate enhanced coastal winter and spring sea ice cover in the 1940s and 1950s and low sea ice cover in the 1960s and 1970s in correspondence with other paleo records (e.g. Abram et al., 2010; Hobbs et al., 2016). A distinct increase in $IPSO_{25}$ and HBI Z-triene concentrations since 1930 CE was also reported by Barbara et al. (2013) on both sides of the AP (supplements S4). We suggest that higher production of $IPSO_{25}$ and sterols could be related to pulses of cold water and nutrients due to glacier retreat (Cook et al., 2016; Kunz et al., 2012). The increasing sea ice cover at all core sites contrasts a reconstructed sea ice decrease from satellite and ice cores since the 1950s for the Bellingshausen Sea (Abram et al., 2010; Hobbs et al., 2016). This contradicting long-term sea ice growth is also evident in the study by Barbara et al. (2013) who first

https://doi.org/10.5194/cp-2020-63
Preprint. Discussion started: 12 May 2020


Climate of the Past Discussions

observed a shortening of the sea ice season but an advance thereafter due to a stable, sea ice favoring environment under mild conditions after 1950 CE.

Unit D: Warm reversal and sea ice peak from 1990 to 2006 CE. The last unit is marked by the trend reversal to a warm subsurface ocean (Cook et al., 2016), present at all core locations in the Bransfield Strait. Sea ice cover tends to increase towards maximum values and seems to reflect recent observations of sea ice cover rebounds in the Bellingshausen Sea and the WAP after 2005 CE (Hobbs et al., 2016; Schofield et al., 2018). Since the last unit is very short, the interpretation of warm ocean temperature together with a high sea ice cover is rather tentative.

We note that for the interpretation of biomarker-based sea ice reconstructions the potential degradation of biomarkers affecting their downcore concentration profile needs to be taken into consideration. We observe that the upper part of the sediment cores contains higher concentrations of $IPSO_{25}$, HBI trienes and sterols compared to the underlying older sediments. A similar pattern in $IPSO_{25}$ and HBI triene concentrations is also reported by Barbara et al. (2013). Their biomarker concentrations from the western AP equal the concentrations in the Bransfield Strait but do not show such high values near the sediment surface, as in our data, are not present. Auto- and photooxidative degradation of $IPSO_{25}$ and HBI trienes was already studied in laboratory experiments (Rontani et al., 2014, 2011) and autoxidative and bacterial degradation was also found in the oxic layers of surface sediments (Rontani et al., 2019). According to these results, a faster degradation of HBI trienes (because of their higher number of double bonds) in the upper centimeters of the herein studied sediment cores would lead to higher $PIPSO_{25}$ values with progressive degradation. Sterols might also undergo degradation (Rontani et al., 2012) but studies from Antarctic sediments are still missing. As we observe remarkably high HBI triene concentrations in core PS97/072-2 in the late 20th century and lower concentrations towards present (Fig. 3, supplements S3), we suggest that degradation does not have major impacts on biomarker concentrations presented in this study.

4.2 Comparison of proxy-derived and modelled sea ice estimates with satellite sea ice observations

We compared $IPSO_{25}$ concentrations, P_ZIPSO_{25} values, and diatom-based WSI estimates with satellite data and with mSSIC to evaluate their accuracy in reflecting spring and winter sea ice cover variability at the core sites over the past 40 years (Fig. 4, supplementary Table 7). Satellite-derived spring sea ice concentrations (satSSIC) show general similarities to fluctuations observed in the $IPSO_{25}$ record indicating lower sea ice cover in the 1980s, a peak in the mid 1990s and a drop in sea ice cover in the early 2000s, except for the coastal remote core site (PS97/072-2) where sea ice concentrations rise towards present (Fig. 4). At the near-coastal core sites (PS97/056-1 and 068-2), these dynamics are well reflected in $IPSO_{25}$ and $PIPSO_{25}$, in particular for site PS97/056-1, where a good correspondence is observed between biomarker and satellite data (Fig. 4). However, we cannot exclude

https://doi.org/10.5194/cp-2020-63
Preprint. Discussion started: 12 May 2020

aliasing effects due to a lower temporal resolution of the sediment cores (Pisias and Mix, 1988). Maximum sea ice concentrations observed in 1996 CE, are well reflected by elevated $IPSO_{25}$ concentrations but the drop afterwards is not that clearly reflected. Diatom-based WSI compared to satellite-derived winter sea ice concentrations (satWSIC) show that these two data sets are in moderate agreement at the near-coastal core sites (PS97/056-1 and PS97/068-2) and winter sea ice coverage seems to be less dynamic at the Peninsula Frontal mixing zone (PS97/068-2). We note that the modelled spring sea ice cover is mostly opposite to satellite data, in particular during the 1990s and 2000s. While modelled and satellite derived data have similar grid sizes (model: 30x30 km, satellite: 25x25 km) we suppose that global models such as AWI-ESM2 cannot resolve the AP sub-aerial and marine topography and have difficulties in capturing local to regional near coastal sea-ice dynamics in the study region. Another reason is related to internal variability and missing feedbacks which makes a direct comparison of short time series difficult. However, both modelled and satellite data show a decreasing trend in spring sea ice cover (about 10%) and a slightly rising trend in winter sea ice cover over the recorded period (about 7%), while sea-ice proxies suggest an increasing trend of spring sea ice. For winters sea ice, core sites PS97/056-1 and PS97/072-2 display a decreasing trend, whereas PS97/068-1 clearly point to an increase of winter sea ice.

For the offshore core site at the East Bransfield Basin (PS97/072-2), $IPSO_{25}$ and $PIPSO_{25}$ correspond better with satSSIC than with mSSIC sea ice data (Fig. 4). Between 1985 and 1995 CE, both $PIPSO_{25}$ indices suggest a similar increase in spring sea ice as the satellite observations. Sea ice estimates from WSI seem to be more related to satSSIC than to satWSIC. Also, WSI estimates are remarkably lower than at the other core sites, although satellite winter sea ice cover is the highest of all. Regarding the oceanographic setting, we consider that also drift ice originating in the Weddell Sea may have affected the deposition of $IPSO_{25}$ at this core site. Input of allochthonous material from the shelf is also possible, which might impact the fidelity of the proxy records.

Based on the overall accordance with satellite data, we conclude that the biomarker and diatom-based sea ice estimations are related to regional dynamics of sea ice cover, as far as we can assess it from the low resolution of the sediment cores. Since HBI Z-trienes and sterol concentration profiles are similar to $IPSO_{25}$ concentrations (Fig. 3, supplements S3) we suggest that sea ice dynamics also promote growth of open marine phytoplankton species due to nutrient release or nutrient upwelling (Sanchez et al., 2019; Vernet et al., 2008). As the record of satellite observations is short, it is not clear if decadal or centennial sea ice trends can be directly derived from our biomarker records. Hence, we use modelled and ice core data for further insights over the full sediment records.

4.3 Comparison of sea ice proxy records with modelled and ice core data covering the pre-satellite era

By comparing $IPSO_{25}$, P_ZIPSO_{25}-based sea ice estimates and WSI with modelled spring sea ice data, we note opposite long-term sea ice trends reflected in the proxy records and the modelled data for the past 240 years (Fig.

https://doi.org/10.5194/cp-2020-63
Preprint. Discussion started: 12 May 2020


Climate of the Past Discussions

5). Modelled spring sea ice concentration and thickness show a clear decreasing trend at all core sites with a loss of sea ice cover between 15% and 20%. Modelled sea ice cover fluctuates strongly at the East Bransfield Basin (PS97/072-2) while the coastal core sites run almost parallel. Although the modelled spring sea ice does not agree with satellite data on local to regional scale (Fig. 4) it does reflect the satellite observations of the large-scale general trend of sea ice decline and warming in the Bellingshausen Sea and at the WAP (Parkinson and Cavalieri, 2012; Vaughan et al., 2003).

The increasing concentrations of $IPSO_{25}$ as well as the rise of both parallel running P_ZIPSO_{25} values and diatom-derived WSI concentrations recorded in all three sediment cores suggest a long-term sea ice advance. On the other hand, the rise in the concentrations of the HBI Z-triene and sterols also rise (supplements S3), which indicates more open marine and/or stable ice edge conditions promoting phytoplankton productivity. We suppose that a thinning of the ice and a hence higher light penetration permitting photosynthesis at the ice-water interface (Hancke et al., 2018) could have triggered the productivity of $IPSO_{25}$ source diatoms. In addition, increased melting of sea could have contributed to a higher deposition of sea ice diatoms and $IPSO_{25}$. Thinner ice and accelerated melting during spring may have resulted in a largely ice-free sea surface during summer promoting phytoplankton (biomarker) productivity. The declining mSSIC and mSSIT (supplements S5) support this interpretation. Increasing concentrations of both $IPSO_{25}$ and phytoplankton-derived biomarker lipids accordingly may reflect more pronounced ice-edge conditions and/or a distinct seasonality in spring and summer conditions at the WAP through the past 200 years.

For the WAP, we generally expect influences of meltwater inputs from glacial melting (Meredith et al., 2018), additional nutrient input from the APCC and intense mixing at the Peninsula Front. As the distribution of $IPSO_{25}$ is sensitive to local oceanographic conditions (Smik et al., 2016a), biomarker-based sea ice studies require an interpretation that takes the specific environmental characteristics of the region into account. Obviously, high fluctuation in sea ice cover, sea ice thickness and water temperature stimulate phytoplankton growth rather than stable conditions with very high and long lasting or low ice covers and/or ice-free sea surface (e.g. Xiao et al., 2013). We hence propose to compare the individual concentration records of $IPSO_{25}$ and phytoplankton biomarkers rather than using the $IPSO_{25}$ (and $PIPSO_{25}$) record alone to deduce sea ice conditions.

We further consider records of MSA, an organic aerosol, which is associated with marine biological activity during sea ice breakup and is used as a proxy for paleo marine productivity and seasonal sea ice reconstructions in ice cores. Influenced by timing, duration and spatial extent of sea ice breakup MSA concentrations are linked with winter sea ice extent in some regions and summer productivity within the sea ice zone in other regions of Antarctica (Thomas et al., 2019 and references therein). Here we use records of MSA from the Dyer Plateau on the AP as

https://doi.org/10.5194/cp-2020-63
Preprint. Discussion started: 12 May 2020


Climate of the Past Discussions

well as a stacked MSA record based on three regional ice cores including Dyer Palteau (Abram et al., 2010) that reflect winter sea ice dynamics in the Bellingshausen Sea. Both records display an overall decreasing trend in MSA concentrations since 1900 CE indicating less sea ice (Fig. 5). The pattern shows some agreement with the mSSIC from the East Bransfield Basin (PS97/072-2) but is opposite to our biomarker records and sea ice indices for all three core sites. This is likely due to the fact that our sediment records reflect local to regional changes strongly influenced by the AP as a geographic barrier and the complex oceanography within the Bransfield Strait from interaction of BSW and WSW. As both the Dyer Plateau and the stacked MSA records are dominated by large-scale winter sea ice cover variability in the Bellingshausen Sea (centered between 70° and 100°W) (Abram et al., 2010), we suggest that the regional sea ice variability within the Bransfield Strait covered by our sediment cores is not well reflected in the ice core records.

Additionally, we took the latitudinal movement of the spring sea ice edge from modelled data (mSSIE, Fig. 5) into account, which displays a southward shift down to 63.5°S reflecting sea ice retreat and proposes the occasional absence of spring sea ice at all core sites since the 1970s. The spatial shift of the sea ice edge must be treated with caution because the model does not account for regional impacts, coastal and peninsula interactions and seasonal input of drift ice from the Weddell Sea. The MSA-based winter sea ice edge (WSIE, Fig. 5) (Abram et al., 2010) displays the same decreasing trend in the Bellingshausen Sea but is located 3° to the south of the modelled ice edge (from 65° to 66°S). The fact that our core sites are located north of this projected WSIE shift is another argument why the ice core MSA cannot be considered to reflect sea ice conditions in our study area, which, according to the ice core data would have been free of sea ice during the entire 20th century.

4.4 Comparison of marine temperature proxy records with model and ice core data

Comparison of GDGT-based temperatures with modelled subsurface ocean temperature mSOT reveals a general disagreement over the 20th century (Fig. 6). Only at the Orleans Trough (PS97/068-2) we assume SOT^{TEX} to reflect atmospheric temperatures due to an enhanced water mixing at the Peninsula Front since the mean temperature of +1.9° C is remarkably higher compared to the other core sites with -0.1° C at PS97/056-1 and -0.6° C at PS97/072-2. During the 19th century, SOT^{TEX}-based cold (around 1850s and 1900 CE) and warm events (from 1860 to 1880 CE, and around 1910 CE), respectively, agree better with mSOT at all core sites than in the 20th century. SOT^{OH} does not correspond to mSOT except since the 1990s when both data sets reflect the modern warming. SSST from diatoms show a short cool period around 1900 CE similar to SOT^{TEX} and modelled data. In general, biomarker derived temperatures point to a slight cooling trend over the last 200 years at the WAP which is contradicted by the mSOT data.

https://doi.org/10.5194/cp-2020-63
Preprint. Discussion started: 12 May 2020


Climate of the Past Discussions
Open Access
EGU

Interestingly, highly variable but continuously increasing mSOT (and mSAT) match with the observed trends in atmospheric warming derived from stable isotope ice core data (Fig. 6). The records of $\delta^{18}O$ records at Bruce Plateau (Goodwin et al., 2016) and δD records from *James Ross Island* (Abram et al., 2013) display the large-scale air temperature evolution in the sector of the Bellingshausen Sea and the Antarctic Peninsula region, and show the same upward trend as air temperatures from several meteorological stations at the WAP (Stastna, 2010). However, we note that ice cores represent a large regional scale and meteorological station records are influenced by e.g. altitude, morphology and local wind patterns, while GDGT-based derived ocean temperatures picture a local to regional marine record controlled by BSW and WSW. We also note that the ocean is decoupled from the atmosphere during periods with sea ice cover and a heating of the ocean by the atmosphere is diminished. Further, sea ice melting in spring enhances the stratification of the upper water column and restricts heat exchange between the subsurface ocean and atmosphere.

4.5 Sea ice evolution and large-scale atmospheric circulation patterns

Since atmospheric circulation affects the heat and sea ice distribution at the WAP especially during spring time (Clem et al., 2016), we expect patterns of ENSO and/or SAM to leave a footprint in our spring sea ice $IPSO_{25}$ record. Several studies suggest an enhanced influence of ENSO and SAM on Antarctic temperatures with increasing greenhouse gas concentrations, so their relation to sea ice is a crucial factor for sea ice and climate predictions (Rahaman et al., 2019; Stammerjohn et al., 2008b). For example, the atmosphere-ocean-sea ice interactions impact the WAP strongly through increased northerly winds during an in-phase -ENSO/+SAM mode. They lead to a strong, positive feedback of atmospheric warming amplification due to shorter sea ice seasons, thinner sea ice cover with more leads and an enhanced heat flux from the ocean (Stammerjohn et al., 2008a).

We compared $IPSO_{25}$ from all core sites with a tree-ring based ENSO reconstruction (Li et al., 2013) and SAM data from proxy records including the full mid-latitude to polar domain of the Drake Passage (Abram et al., 2014) (Fig. 7). Both, ENSO and SAM, have oscillating positive and negative periods and SAM shows a slight decrease until 1860 CE. Since 1930 CE, SAM, and since 1960 CE, ENSO, increase again and reach maximum positive states in the 2000s. When comparing biomarker and circulation patterns, SAM matches best with elevated HBI concentrations, especially at the coastal core sites, relating a higher accumulation of $IPSO_{25}$ with a +SAM. During a +SAM, stronger westerlies lead to a southward shift of the low-pressure cell over the Bellingshausen Sea and the strengthening of the polar frontal jet (Marshall et al., 2006). The blocking effect of the AP is diminished because air masses pass over the northern AP from west to east (Marshall et al., 2006). This results in a remarkable impact on rising summer air temperatures on the eastern AP leeside due to a "Föhn" effect (Klemp and Lilly, 1975). In contrast, the temperature effects on the western AP are very small and not even detectable at e.g. the

https://doi.org/10.5194/cp-2020-63
Preprint. Discussion started: 12 May 2020


Climate of the Past Discussions

southwest Vernadsky/Faraday Station (Marshall et al., 2006). Nevertheless, our records suggest that a +SAM is positively related to the production of $IPSO_{25}$ and HBI Z-triene at the WAP, especially since the mid 20th century. The pattern of ENSO is related negatively with biomarker concentrations in the 19th century (especially at core site PS97/072-2) and more positively in the 20th century. The recent shift to a positive ENSO is accompanied by increased $IPSO_{25}$ concentrations. After Yuan (2004) a +ENSO causes sea ice advance under cold conditions in the Weddell Sea and the WAP, and warm, moist conditions in the Southern Pacific Ocean. However, due to observations of recently rising atmospheric temperature (Stastna, 2010), ocean temperature (Cook et al., 2016) and declining sea ice cover, a +ENSO seems to be more likely related to warm and sea ice reduced conditions at the WAP in the studied period. Nevertheless, we observe that the $IPSO_{25}$ production at the coastal core sites (PS97/056-1 and 068-1) correspond to ENSO since the 1980s. While neither SAM nor ENSO alone seem to exert a consistent control on $IPSO_{25}$ and phytoplankton production at the WAP, +ENSO together with +SAM seem to be linked to higher $IPSO_{25}$ concentrations especially in the 20th century, which agrees with previous suggestions regarding the impact of atmospheric circulation pattern on sea ice conditions (Barbara et al., 2013; Etourneau et al., 2013).

5 Summary and Conclusions

In this study we analyzed the spring sea ice biomarker $IPSO_{25}$ and other organic biomarkers as well as diatom assemblages in three sediment cores from the Western Antarctic Peninsula region covering the industrial era and combined them with numerical model data, satellite observations, temperature records and paleo records of atmospheric circulation patterns. We note that the interpretation of the biomarker data for past sea ice estimates in Antarctica is strongly impacted by the origin of water masses and mixing, nutrient input and dynamics of sea ice-related primary production. Based on sea ice biomarkers and sea ice indices, the 200-year records can be divided into four units:

Unit A Before 1850 CE, the sea ice cover in the WAP was moderate with a low primary productivity and low seasonal sea ice variability influenced by WSW inflow into the Bransfield Strait.

Unit B From 1850 to 1930 CE, low to moderate stable sea ice cover was common at the coastal WAP, while rapid changes in sea ice seasonality were evident at the East Bransfield Basin due to changes in oceanographic pattern and enhanced BSW inflow.

Unit C 1930 CE marked a turning point in sea ice cover with increased sea ice dynamics triggering melting and primary production of both open marine and sea ice species, with periods of high (1940s-1950s) and low sea ice cover (1960s-1970s).

https://doi.org/10.5194/cp-2020-63
Preprint. Discussion started: 12 May 2020


Climate of the Past Discussions

Unit D Since 1990 CE, the anthropogenic warming reversal is evident in subsurface ocean temperatures and low sea ice cover with high seasonal dynamics promoting marine production and causing maximum sea ice indices.

While $IPSO_{25}$ concentrations agree with satellite sea ice data, they seem to contradict with long-term large-scale ice core and model data. We explain this as a result of local coastal influences, high sea ice dynamics and thinner sea ice promoting the production of both sea ice diatoms and open marine phytoplankton affecting the interpretation of $IPSO_{25}$ and the sea ice index $PIPSO_{25}$. When estimating spring sea ice cover, the strong susceptibility of $IPSO_{25}$ to local influences such as water masses, coastal interaction and, e.g. a higher sea ice algae productivity resulting from thinner ice cover need to be taken into account. We hence recommend to consider additional phytoplankton data instead of constructing sea ice estimates on $IPSO_{25}$ and $PIPSO_{25}$ records solely. We do not observe a relation between ocean temperature evolution and retreating sea ice in the 20th century. The examination of ENSO and SAM paleo records reveals that both seem to affect the sea ice regime at the WAP and that SAM in particular could be a main driver for sea ice conditions favoring $IPSO_{25}$ production.

https://doi.org/10.5194/cp-2020-63
Preprint. Discussion started: 12 May 2020

Climate of the Past Discussions

Data Availability

All data will be available at the open access repository www.pangaea.de.

Author contributions

The study was conceived by MV and JM. Data collections and experimental investigations were done by MV together with PC, LR, PM and CBL (diatoms, dating), WG (dating), OE (diatom transfer functions), JM and GM (HBIs, GDGTs), XS and GL (modelling and supplement Fig. S2), CH (satellite sea ice data), and TO (ice cores). MV drafted the manuscript and figures. JM supervised the study. All authors contributed to the interpretation and discussion of the results and the conclusion of this study.

Competing interests

None of the authors has a conflict of interest.

Acknowledgement

We thank the captain, crew and chief scientist Frank Lamy of RV Polarstern cruise PS97. Denise Diekstall, Jens Hefter, Ingrid Stimac and Ruth Cordelair are thanked for their laboratory support. We also thank Andrés Cádiz for the help on diatom slide preparations and counts on core PS97/056-1. Simon Belt is acknowledged for providing the 7-HND internal standard for HBI quantification. Financial support was provided through the Helmholtz Research grant VH-NG-1101 and the Helmholtz Excellence Network "The Polar System and its Effects on the Ocean Floor" ExNet-0001. Partial support from IDEAL Center grant FONDAP 15150003, Chile, is acknowledged.

https://doi.org/10.5194/cp-2020-63
Preprint. Discussion started: 12 May 2020

References

Abram, N. J., Thomas, E. R., McConnell, J. R., Mulvaney, R., Bracegirdle, T. J., Sime, L. C. and Aristarain, A. J.: Ice core evidence for a 20th century decline of sea ice in the Bellingshausen Sea, Antarctica, J. Geophys. Res., 115(D23), D23101, doi:10.1029/2010JD014644, 2010.

Abram, N. J., Mulvaney, R., Wolff, E. W., Triest, J., Kipfstuhl, S., Trusel, L. D., Vimeux, F., Fleet, L. and Arrowsmith, C.: Acceleration of snow melt in an Antarctic Peninsula ice core during the twentieth century, Nat. Geosci., 6(5), 404–411, doi:10.1038/ngeo1787, 2013.

Abram, N. J., Mulvaney, R., Vimeux, F., Phipps, S. J., Turner, J. and England, M. H.: Evolution of the Southern Annular Mode during the past millennium, Nat. Clim. Chang., 4(7), 564–569, doi:10.1038/nclimate2235, 2014.

Abram, N. J., McGregor, H. V, Tierney, J. E., Evans, M. N., McKay, N. P. and Kaufman, D. S.: Early onset of industrial-era warming across the oceans and continents, Nature, 536(7617), 411–418, doi:10.1038/nature19082, 2016.

Alexander, V. and Niebauer, H. J.: Oceanography of the eastern Bering Sea ice-edge zone in spring, Limn, 26(6), 1111–1125 [online] Available from: http://doi.wiley.com/10.1029/2007RG000250, 1981.

Allen, C. S.: Proxy development: a new facet of morphological diversity in the marine diatom Eucampia antarctica (Castracane) Mangin, J. Micropalaeontology, 33(2), 131–142, doi:10.1144/jmpaleo2013-025, 2014.

Allison, I., Tivendale, C. M., Akerman, G. J., Tann, J. M. and Wills, R. H.: Seasonal Variations In The Surface Energy Exchanges Over Antarctic Sea Ice and Coastal Waters, Ann. Glaciol., 3, 12–16, doi:10.3189/S0260305500002445, 1982.

Appleby, P. G. and Oldfield, F.: The calculation of lead-210 dates assuming a constant rate of supply of unsupported 210Pb to the sediment, CATENA, 5(1), 1–8, doi:10.1016/S0341-8162(78)80002-2, 1978.

Armand, L. K. and Zielinski, U.: Diatom Species of the genus Rhizosolenia from Southern Ocean sediments: distribution and taxonomic notes, Diatom Res., 16(2), 259–294, doi:10.1080/0269249X.2001.9705520, 2001.

Arrigo, K. R., Worthen, D. L., Lizotte, M. P., Dixon, P. and Dieckmann, G. S.: Primary Production in Antarctic Sea Ice, Science (80-.)., 276(5311), 394–397, doi:10.1126/science.276.5311.394, 1997.

Barbara, L., Crosta, X., Schmidt, S. and Massé, G.: Diatoms and biomarkers evidence for major changes in sea ice conditions prior the instrumental period in Antarctic Peninsula, Quat. Sci. Rev., 79, 99–110, doi:10.1016/j.quascirev.2013.07.021, 2013.

Belt, S. T. and Müller, J.: The Arctic sea ice biomarker IP 25 : a review of current understanding , recommendations for future research and applications in palaeo sea ice reconstructions, Quat. Sci. Rev., 79, 9–25, doi:10.1016/j.quascirev.2012.12.001, 2013.

https://doi.org/10.5194/cp-2020-63
Preprint. Discussion started: 12 May 2020

710 Belt, S. T., Allard, W. G., Massé, G., Robert, J.-M. and Rowland, S. J.: Highly branched isoprenoids (HBIs): identification of the most common and abundant sedimentary isomers, Geochim. Cosmochim. Acta, 64(22), 3839–3851, doi:10.1016/S0016-7037(00)00464-6, 2000.

Belt, S. T., Brown, T. A., Ringrose, A. E., Cabedo-Sanz, P., Mundy, C. J., Gosselin, M. and Poulin, M.: Quantitative measurement of the sea ice diatom biomarker IP25 and sterols in Arctic sea ice and underlying 715 sediments: Further considerations for palaeo sea ice reconstruction, Org. Geochem., 62, 33–45, doi:10.1016/J.ORGGEOCHEM.2013.07.002, 2013.

Belt, S. T., Smik, L., Brown, T. A., Kim, J. H., Rowland, S. J., Allen, C. S., Gal, J. K., Shin, K. H., Lee, J. I. and Taylor, K. W. R.: Source identification and distribution reveals the potential of the geochemical Antarctic sea ice proxy IPSO25, Nat. Commun., 7, 1–10, doi:10.1038/ncomms12655, 2016.

720 Belt, S. T., Brown, T. A., Smik, L., Tatarek, A., Wiktor, J., Stowasser, G., Assmy, P., Allen, C. S. and Husum, K.: Identification of C25 highly branched isoprenoid (HBI) alkenes in diatoms of the genus Rhizosolenia in polar and sub-polar marine phytoplankton, Org. Geochem., 110, 65–72, doi:10.1016/j.orggeochem.2017.05.007, 2017.

Belt, S. T. T., Brown, T. A. A., Ampel, L., Cabedo-Sanz, P., Fahl, K., Kocis, J. J. J., Massé, G., Navarro-Rodriguez, A., Ruan, J. and Xu, Y.: An inter-laboratory investigation of the Arctic sea ice biomarker proxy IP25 in marine 725 sediments: key outcomes and recommendations, Clim. Past, 10(1), 155–166, doi:10.5194/cp-10-155-2014, 2014.

Berger, A. L.: Long-Term Variations of Daily Insolation and Quaternary Climate Changes, J. Atmos. Sci., 35, 2362–2367, 1978.

Bevington, P. R., Robinson, D. K. and Bunce, G.: Data Reduction and Error Analysis for the Physical Sciences, 2nd Edition, American Association of Physics Teachers., 1993.

730 Blaauw, M.: Methods and code for 'classical' age-modelling of radiocarbon sequences, Quat. Geochronol., 5(5), 512–518, doi:10.1016/J.QUAGEO.2010.01.002, 2010.

Bracegirdle, T. J., Stephenson, D. B., Turner, J. and Phillips, T.: The importance of sea ice area biases in 21st century multimodel projections of Antarctic temperature and precipitation, Geophys. Res. Lett., 42(24), 10,810-832,839, doi:10.1002/2015GL067055, 2015.

735 Bracegirdle, T. J., Colleoni, F., Abram, N. J., Bertler, N. A. N., Dixon, D. A., England, M., Favier, V., Fogwill, C. J., Fyfe, J. C., Goodwin, I., Goosse, H., Hobbs, W., Jones, J. M., Keller, E. D., Khan, A. L., Phipps, S. J., Raphael, M. N., Russell, J., Sime, L., Thomas, E. R., van den Broeke, M. R. and Wainer, I.: Back to the Future: Using Long-Term Observational and Paleo-Proxy Reconstructions to Improve Model Projections of Antarctic Climate, Geosciences, 9(6), 255, doi:10.3390/geosciences9060255, 2019.

740 Buffen, A., Leventer, A., Rubin, A. and Hutchins, T.: Diatom assemblages in surface sediments of the

https://doi.org/10.5194/cp-2020-63
Preprint. Discussion started: 12 May 2020

northwestern Weddell Sea, Antarctic Peninsula, Mar. Micropaleontol., 62(1), 7–30, doi:10.1016/J.MARMICRO.2006.07.002, 2007.

Burckle, L. H. and Cooke, D. W.: Late Pleistocene Eucampia antarctica Abundance Stratigraphy in the Atlantic Sector of the Southern Ocean, Micropaleontology, 29(1), 6, doi:10.2307/1485648, 1983.

Butterworth, B. J. and Miller, S. D.: Air-sea exchange of carbon dioxide in the Southern Ocean and Antarctic marginal ice zone, Geophys. Res. Lett., 43(13), 7223–7230, doi:10.1002/2016GL069581, 2016.

Campagne, P., Crosta, X., Schmidt, S., Noëlle Houssais, M., Ther, O. and Massé, G.: Sedimentary response to sea ice and atmospheric variability over the instrumental period off Adélie Land, East Antarctica, Biogeosciences, 13(14), 4205–4218, doi:10.5194/bg-13-4205-2016, 2016.

Canals, M. and Amblas, D.: Seafloor kettle holes in Orleans Trough, Bransfield Basin, Antarctic Peninsula, Geol. Soc. London, Mem., 46(1), 313–314, doi:10.1144/M46.16, 2016a.

Canals, M. and Amblas, D.: The bundle: a mega-scale glacial landform left by an ice stream, Western Bransfield Basin, Geol. Soc. London, Mem., 46(1), 177–178, doi:10.1144/M46.157, 2016b.

Canals, M., Amblas, D. and Casamor, J. L.: Cross-shelf troughs in Central Bransfield Basin, Antarctic Peninsula, Geol. Soc. London, Mem., 46(1), 171–172, doi:10.1144/M46.138, 2016.

Cárdenas, P., Lange, C. B., Vernet, M., Esper, O., Srain, B., Vorrath, M.-E. M.-E., Ehrhardt, S., Müller, J., Kuhn, G., Arz, H. W. H. W. H. W., Lembke-Jene, L., Lamy, F. and Paola Cárdenas, Carina B. Lange, Maria Vernet, Oliver Esper, Benjamin Srain, Maria-Elena Vorrath, Sophie Ehrhardt, Juliane Müller, Gerhard Kuhn, Helge W.Arz, Lester Lembke-Jene, F. L.: Biogeochemical proxies and diatoms in surface sediments across the Drake Passage reflect oceanic domains and frontal systems in the region, Prog. Oceanogr., 174, 72–88, doi:10.1016/j.pocean.2018.10.004, 2019.

Cavalieri, D. J., Parkinson, C. L., Gloersen, P. and Zwally, H. J.: Sea Ice Concentrations from Nimbus-7 SMMR and DMSP SSM/I-SSMIS Passive Microwave Data, Version 1, Boulder, Color. USA, doi:10.5067/8GQ8LZQVL0VL, 1996.

Cefarelli, A. O., Ferrario, M. E., Almandoz, G. O., Atencio, A. G., Akselman, R. and Vernet, M.: Diversity of the diatom genus Fragilariopsis in the Argentine Sea and Antarctic waters: morphology, distribution and abundance, Polar Biol., 33(11), 1463–1484, doi:10.1007/s00300-010-0794-z, 2010.

Clem, K. R., Renwick, J. A., McGregor, J. and Fogt, R. L.: The relative influence of ENSO and SAM on Antarctic Peninsula climate, J. Geophys. Res. Atmos., 121(16), 9324–9341, doi:10.1002/2016JD025305, 2016.

Collares, L. L., Mata, M. M., Kerr, R., Arigony-Neto, J. and Barbat, M. M.: Iceberg drift and ocean circulation in the northwestern Weddell Sea, Antarctica, Deep Sea Res. Part II Top. Stud. Oceanogr., 149(January 2019), 10–

https://doi.org/10.5194/cp-2020-63
Preprint. Discussion started: 12 May 2020

24, doi:10.1016/j.dsr2.2018.02.014, 2018.

Cook, A. J., Holland, P. R., Meredith, M. P., Murray, T., Luckman, A. and Vaughan, D. G.: Ocean forcing of glacier retreat in the western Antarctic Peninsula, Science (80-.)., 353(6296), 283–286, doi:10.1126/science.aae0017, 2016.

Crosta, X., Pichon, J.-J. and Burckle, L. H.: Application of modern analog technique to marine Antarctic diatoms: Reconstruction of maximum sea-ice extent at the Last Glacial Maximum, Paleoceanography, 13(3), 284–297, doi:10.1029/98PA00339, 1998.

Crosta, X., Sturm, A., Armand, L. and Pichon, J.-J.: Late Quaternary sea ice history in the Indian sector of the Southern Ocean as recorded by diatom assemblages, Mar. Micropaleontol., 50(3–4), 209–223, doi:10.1016/S0377-8398(03)00072-0, 2004.

Danilov, S., Sidorenko, D., Wang, Q. and Jung, T.: The Finite-volumE Sea ice–Ocean Model (FESOM2), Geosci. Model Dev., 10(2), 765–789, doi:10.5194/gmd-10-765-2017, 2017.

Ding, Q., Steig, E. J., Battisti, D. S. and Wallace, J. M.: Influence of the tropics on the southern annular mode, J. Clim., 25(18), 6330–6348, doi:10.1175/JCLI-D-11-00523.1, 2012.

Esper, O. and Gersonde, R.: New tools for the reconstruction of Pleistocene Antarctic sea ice, Palaeogeogr. Palaeoclimatol. Palaeoecol., 399, 260–283, doi:10.1016/J.PALAEO.2014.01.019, 2014a.

Esper, O. and Gersonde, R.: Quaternary surface water temperature estimations: New diatom transfer functions for the Southern Ocean, Palaeogeogr. Palaeoclimatol. Palaeoecol., 414, 1–19, doi:10.1016/J.PALAEO.2014.08.008, 2014b.

Esper, O., Gersonde, R. and Kadagies, N.: Diatom distribution in southeastern Pacific surface sediments and their relationship to modern environmental variables, Palaeogeogr. Palaeoclimatol. Palaeoecol., 287(1–4), 1–27, 2010.

Etourneau, J., Collins, L. G., Willmott, V., Kim, J. H., Barbara, L., Leventer, A., Schouten, S., Sinninghe Damsté, J. S., Bianchini, A., Klein, V., Crosta, X. and Massé, G.: Holocene climate variations in the western Antarctic Peninsula: Evidence for sea ice extent predominantly controlled by changes in insolation and ENSO variability, Clim. Past, 9(4), 1431–1446, doi:10.5194/cp-9-1431-2013, 2013.

Etourneau, J., Sgubin, G., Crosta, X., Swingedouw, D., Willmott, V., Barbara, L., Houssais, M. N., Schouten, S., Damsté, J. S. S., Goosse, H., Escutia, C., Crespin, J., Massé, G. and Kim, J. H.: Ocean temperature impact on ice shelf extent in the eastern Antarctic Peninsula, Nat. Commun., 10(1), 8–15, doi:10.1038/s41467-018-08195-6, 2019.

Fietz, S., Huguet, C., Rueda, G., Hambach, B. and Rosell-Melé, A.: Hydroxylated isoprenoidal GDGTs in the Nordic Seas, Mar. Chem., 152, 1–10, doi:10.1016/j.marchem.2013.02.007, 2013.

https://doi.org/10.5194/cp-2020-63
Preprint. Discussion started: 12 May 2020

Flynn, W. W.: The determination of low levels of polonium-210 in environmental materials, Anal. Chim. Acta, 43(C), 221–227, doi:10.1016/S0003-2670(00)89210-7, 1968.

Gersonde, R. and Zielinski, U.: The reconstruction of late Quaternary Antarctic sea-ice distribution — the use of diatoms as a proxy for sea-ice, Palaeogeogr. Palaeoclimatol. Palaeoecol., 162, 263–286, doi:10.1016/S0031-0182(00)00131-0, 2000.

Gersonde, R., Crosta, X., Abelmann, A. and Armand, L.: Sea-surface temperature and sea ice distribution of the Southern Ocean at the EPILOG Last Glacial Maximum—a circum-Antarctic view based on siliceous microfossil records, Quat. Sci. Rev., 24(7–9), 869–896, doi:10.1016/J.QUASCIREV.2004.07.015, 2005.

Gloersen, P., Campbell, W. J., Cavalieri, D. J., Comiso, J. C., Parkinson, C. L. and Zwally, H. J.: Arctic and antarctic sea ice, 1978, Ann. Glaciol., 17, 149–154, 1993.

Gonçalves-Araujo, R., de Souza, M. S., Tavano, V. M. and Garcia, C. A. E.: Influence of oceanographic features on spatial and interannual variability of phytoplankton in the Bransfield Strait, Antarctica, J. Mar. Syst., 142, 1–15, doi:10.1016/J.JMARSYS.2014.09.007, 2015.

Goodwin, B. P., Mosley-Thompson, E., Wilson, A. B., Porter, S. E. and Sierra-Hernandez, M. R.: Accumulation Variability in the Antarctic Peninsula: The Role of Large-Scale Atmospheric Oscillations and Their Interactions, J. Clim., 29(7), 2579–2596, doi:10.1175/JCLI-D-15-0354.1, 2016.

Hancke, K., Lund-Hansen, L. C., Lamare, M. L., Højlund Pedersen, S., King, M. D., Andersen, P. and Sorrell, B. K.: Extreme Low Light Requirement for Algae Growth Underneath Sea Ice: A Case Study From Station Nord, NE Greenland, J. Geophys. Res. Ocean., 123(2), 985–1000, doi:10.1002/2017JC013263, 2018.

Hellmer, H. H., Kauker, F., Timmermann, R., Determann, J. and Rae, J.: Twenty-first-century warming of a large Antarctic ice-shelf cavity by a redirected coastal current, Nature, 485(7397), 225–228, doi:10.1038/nature11064, 2012.

Hobbs, W. R., Massom, R., Stammerjohn, S., Reid, P., Williams, G. and Meier, W.: A review of recent changes in Southern Ocean sea ice , their drivers and forcings, Glob. Planet. Change, 143, 228–250, doi:10.1016/j.gloplacha.2016.06.008, 2016.

Hofmann, E. E., Klinck, J. M., Lascara, C. M. and Smith, D. A.: Water mass distribution and circulation west of the Antarctic Peninsula and including Bransfield Strait, in Foundations for Ecological Research West of the Antarctic Peninsula, edited by R. M. Ross, E. E. Hofmann, and L. B. Quetin, pp. 61–80, American Geophysical Union (AGU), Washington, D. C., 1996.

Hopmans, E. C., Weijers, J. W. H., Schefuß, E., Herfort, L., Sinninghe Damsté, J. S. and Schouten, S.: Variability in the Benguela Current upwelling system over the past 70,000 years, Earth Planet. Sci. Lett., 224(1–2), 107–116,

https://doi.org/10.5194/cp-2020-63
Preprint. Discussion started: 12 May 2020

doi:10.1016/j.epsl.2004.05.012, 2004.

Huss, M. and Farinotti, D.: A high-resolution bedrock map for the Antarctic Peninsula, Cryosph., 8(4), 1261–1273, doi:10.5194/tc-8-1261-2014, 2014.

Ingólfsson, Ó., Hjort, C. and Humlum, O.: Glacial and Climate History of the Antarctic Peninsula since the Last Glacial Maximum, Arctic, Antarct. Alp. Res., 35(2), 175–186, doi:10.1657/1523-0430(2003)035[0175:GACHOT]2.0.CO;2, 2003.

IPCC: Summary for Policymakers, in Global Warming of 1.5°C. An IPCC Special Report on the impacts of global warming of 1.5°C above pre-industrial levels and related global greenhouse gas emission pathways, in the context of strengthening the global response to the threat of climate change, edited by V. Masson-Delmotte, P. Zhai, H.-O. Pörtner, D. Roberts, J. Skea, P. R. Shukla, A. Pirani, W. Moufouma-Okia, C. Péan, R. Pidcock, S. Connors, J. B. R. Matthews, Y. Chen, X. Zhou, M. I. Gomis, E. Lonnoy, T. Maycock, M. Tignor, and T. Waterfield, p. 24. [online] Available from: https://www.ipcc.ch/site/assets/uploads/sites/2/2019/05/SR15_SPM_version_report_LR.pdf, 2018.

IPCC: Summary for Policymakers, in IPCC Special Report on the Ocean and Cryosphere in a Changing Climate, edited by H. O. Pörtner, D. C. Roberts, V. Masson-Delmotte, P. Zhai, M. Tignor, E. Poloczanska, K. Mintebeck, M. Nicolai, A. Okem, J. Petzold, B. Rama, and N. Weyer, p. 42. [online] Available from: https://report.ipcc.ch/srocc/pdf/SROCC_SPM_Approved.pdf, 2019.

Jones, J. M., Gille, S. T., Goosse, H., Abram, N. J., Canziani, P. O., Charman, D. J., Clem, K. R., Crosta, X., de Lavergne, C., Eisenman, I., England, M. H., Fogt, R. L., Frankcombe, L. M., Marshall, G. J., Masson-Delmotte, V., Morrison, A. K., Orsi, A. J., Raphael, M. N., Renwick, J. A., Schneider, D. P., Simpkins, G. R., Steig, E. J., Stenni, B., Swingedouw, D. and Vance, T. R.: Assessing recent trends in high-latitude Southern Hemisphere surface climate, Nat. Clim. Chang., 6(10), 917–926, doi:10.1038/nclimate3103, 2016.

Kalanetra, K. M., Bano, N. and Hollibaugh, J. T.: Ammonia-oxidizing Archaea in the Arctic Ocean and Antarctic coastal waters, Environ. Microbiol., 11(9), 2434–2445, doi:10.1111/j.1462-2920.2009.01974.x, 2009.

Kim, D., Kim, D. Y., Kim, Y. J., Kang, Y. C. and Shim, J.: Downward fluxes of biogenic material in Bransfield Strait, Antarctica, Antarct. Sci., 16(3), 227–237, doi:10.1017/S0954102004002032, 2004.

Kim, J.-H., van der Meer, J., Schouten, S., Helmke, P., Willmott, V., Sangiorgi, F., Koç, N., Hopmans, E. C. and Damsté, J. S. S.: New indices and calibrations derived from the distribution of crenarchaeal isoprenoid tetraether lipids: Implications for past sea surface temperature reconstructions, Geochim. Cosmochim. Acta, 74(16), 4639–4654, doi:10.1016/j.gca.2010.05.027, 2010.

Kim, J.-H., Crosta, X., Willmott, V., Renssen, H., Bonnin, J., Helmke, P., Schouten, S. and Sinninghe Damsté, J.

https://doi.org/10.5194/cp-2020-63
Preprint. Discussion started: 12 May 2020

S.: Holocene subsurface temperature variability in the eastern Antarctic continental margin, Geophys. Res. Lett., 39(6), doi:10.1029/2012GL051157, 2012.

Klemp, J. B. and Lilly, D. R.: The Dynamics of Wave-Induced Downslope Winds, J. Atmos. Sci., 32(2), 320–339, doi:10.1175/1520-0469(1975)032<0320:TDOWID>2.0.CO;2, 1975.

Klunder, M. B., Laan, P., De Baar, H. J. W., Middag, R., Neven, I. and Van Ooijen, J.: Dissolved Fe across the Weddell Sea and Drake Passage: impact of DFe on nutrient uptake, Biogeosciences, 11(3), 651–669, doi:10.5194/bg-11-651-2014, 2014.

Kunz, M., King, M. A., Mills, J. P., Miller, P. E., Fox, A. J., Vaughan, D. G. and Marsh, S. H.: Multi-decadal glacier surface lowering in the Antarctic Peninsula, Geophys. Res. Lett., 39(19), n/a--n/a, doi:10.1029/2012GL052823, 2012.

Lamping, N., Müller, J., Esper, O., Hillenbrand, C., Smith, J. A. and Kuhn, G.: Highly branched isoprenoids reveal onset of deglaciation followed by dynamic sea-ice conditions in the western Amundsen Sea, Antarctica, Quat. Sci. Rev., 228, 106103, doi:10.1016/j.quascirev.2019.106103, 2020.

Lamy, F.: The expedition PS97 of the research vessel POLARSTERN to the Drake Passage in 2016, Reports Polar Mar. Res., 7'01, 1–571, doi:10.2312/BzPM_0702_2016, 2016.

Leventer, A.: The fate of Antarctic “sea ice diatoms” and their use as paleoenvironmental indicators, in Antarctic Research Series, edited by M. P. Lizotte and K. R. Arrigo, pp. 121–137, American Geophysical Union (AGU)., 1998.

Li, J., Xie, S.-P., Cook, E. R., Morales, M. S., Christie, D. A., Johnson, N. C., Chen, F., D’Arrigo, R., Fowler, A. M., Gou, X. and Fang, K.: El Niño modulations over the past seven centuries, Nat. Clim. Chang., 3(9), 822–826, doi:10.1038/nclimate1936, 2013.

Liu, J., Curry, J. A. and Martinson, D. G.: Interpretation of recent Antarctic sea ice variability, Geophys. Res. Lett., 31(2), 2000–2003, doi:10.1029/2003GL018732, 2004.

Lorenz, S. J. and Lohmann, G.: Acceleration technique for Milankovitch type forcing in a coupled atmosphere-ocean circulation model: Method and application for the Holocene, Clim. Dyn., 23(7–8), 727–743, doi:10.1007/s00382-004-0469-y, 2004.

Lü, X., Liu, X. L., Elling, F. J., Yang, H., Xie, S., Song, J., Li, X., Yuan, H., Li, N. and Hinrichs, K. U.: Hydroxylated isoprenoid GDGTs in Chinese coastal seas and their potential as a paleotemperature proxy for mid-to-low latitude marginal seas, Org. Geochem., 89–90, 31–43, doi:10.1016/j.orggeochem.2015.10.004, 2015.

Marshall, G. J., Orr, A., van Lipzig, N. P. M. and King, J. C.: The Impact of a Changing Southern Hemisphere Annular Mode on Antarctic Peninsula Summer Temperatures, J. Clim., 19(20), 5388–5404,

https://doi.org/10.5194/cp-2020-63
Preprint. Discussion started: 12 May 2020

doi:10.1175/JCLI3844.1, 2006.

Martinson, D. G. and McKee, D. C.: Transport of warm Upper Circumpolar Deep Water onto the western Antarctic Peninsula continental shelf, Ocean Sci., 8(4), 433–442, doi:10.5194/os-8-433-2012, 2012.

Massé, G., Belt, S. T., Crosta, X., Schmidt, S., Snape, I., Thomas, D. N. and Rowland, S. J.: Highly branched isoprenoids as proxies for variable sea ice conditions in the Southern Ocean, Antarct. Sci., 23(05), 487–498, doi:10.1017/S0954102011000381, 2011.

Meijers, A. J. S., Meredith, M. P., Abrahamsen, E. P., Morales Maqueda, M. A., Jones, D. C. and Naveira Garabato, A. C.: Wind-driven export of Weddell Sea slope water, J. Geophys. Res. Ocean., 121(10), 7530–7546, doi:10.1002/2016JC011757, 2016.

Meinshausen, M., Smith, S. J., Calvin, K., Daniel, J. S., Kainuma, M. L. T., Lamarque, J.-F., Matsumoto, K., Montzka, S. A., Raper, S. C. B., Riahi, K., Thomson, A., Velders, G. J. M. and van Vuuren, D. P. P. P.: The RCP greenhouse gas concentrations and their extensions from 1765 to 2300, Clim. Change, 109(1–2), 213–241, doi:10.1007/s10584-011-0156-z, 2011.

Meredith, M. P. and King, J. C.: Rapid climate change in the ocean west of the Antarctic Peninsula during the second half of the 20th century, Geophys. Res. Lett., 32(19), 1–5, doi:10.1029/2005GL024042, 2005.

Meredith, M. P., Falk, U., Bers, A. V., Mackensen, A., Schloss, I. R., Barlett, E. R., Jerosch, K., Busso, A. S. and Abele, D.: Anatomy of a glacial meltwater discharge event in an Antarctic cove, Philos. Trans. R. Soc. A Math. Phys. Eng. Sci., 376(2122), doi:10.1098/rsta.2017.0163, 2018.

Moffat, C. and Meredith, M.: Shelf-ocean exchange and hydrography west of the Antarctic Peninsula: A review, Philos. Trans. R. Soc. A Math. Phys. Eng. Sci., 376(2122), doi:10.1098/rsta.2017.0164, 2018.

Müller, J., Wagner, A., Fahl, K., Stein, R., Prange, M. and Lohmann, G.: Towards quantitative sea ice reconstructions in the northern North Atlantic: A combined biomarker and numerical modelling approach, Earth Planet. Sci. Lett., 306(3–4), 137–148, doi:10.1016/J.EPSL.2011.04.011, 2011.

Nicholls, K. W., Østerhus, S., Makinson, K., Gammelsrød, T. and Fahrbach, E.: Ice-ocean processes over the continental shelf of the southern Weddell Sea, Antarctica: A review, Rev. Geophys., 47(3), RG3003, doi:10.1029/2007RG000250, 2009.

Nichols, P. D., Volkman, J. K., Palmisano, A. C., Smith, G. A. and White, D. C.: Occurrence of an Isoprenoid C25 diunsaturated alkene and high neutral lipid content in Antarctic Sea-Ice Diatom communities, J. Phycol., 24, 90–96, 1988.

Oksanen, J., Blanchet, F. G., Kindt, R., Legendre, P., Minchin, P. R., O´Hara, R. B., Simpson, G. L., Solymos, P., Stevens, M. H. H. and Wagner, H.: Vegan: Community Ecology Package (R Package Version 2.0-3), 2012.

https://doi.org/10.5194/cp-2020-63
Preprint. Discussion started: 12 May 2020

Otto-Bliesner, B. L., Braconnot, P., Harrison, S. P., Lunt, D. J., Abe-Ouchi, A., Albani, S., Bartlein, P. J., Capron, E., Carlson, A. E., Dutton, A., Fischer, H., Goelzer, H., Govin, A., Haywood, A., Joos, F., LeGrande, A. N., Lipscomb, W. H., Lohmann, G., Mahowald, N., Nehrbass-Ahles, C., Pausata, F. S. R., Peterschmitt, J.-Y. Y., Phipps, S. J., Renssen, H. and Zhang, Q.: The PMIP4 contribution to CMIP6 - Part 2: Two interglacials, scientific objective and experimental design for Holocene and Last Interglacial simulations, Geosci. Model Dev., 10(11), 3979–4003, doi:10.5194/gmd-10-3979-2017, 2017.

Park, E., Hefter, J., Fischer, G., Iversen, M. H., Ramondenc, S., Nöthig, E.-M. and Mollenhauer, G.: Seasonality of archaeal lipid flux and GDGT-based thermometry in sinking particles of high-latitude oceans: Fram Strait (79° N) and Antarctic Polar Front (50° S), Biogeosciences, 16(11), 2247–2268, doi:10.5194/bg-16-2247-2019, 2019.

Parkinson, C. L.: Trends in the length of the Southern Ocean sea-ice season, 1979-99, Ann. Glaciol., 34(1), 435–440, doi:10.3189/172756402781817482, 2002.

Parkinson, C. L.: A 40-y record reveals gradual Antarctic sea ice increases followed by decreases at rates far exceeding the rates seen in the Arctic, Proc. Natl. Acad. Sci., 116(29), 14414–14423, doi:10.1073/pnas.1906556116, 2019.

Parkinson, C. L. and Cavalieri, D. J.: Antarctic sea ice variability and trends, 1979–2010, Cryosph., 6, 871–880, doi:10.5194/tc-6-871-2012, 2012.

Pisias, N. G. and Mix, A. C.: Aliasing of the geologic record and the search for long-period Milankovitch cycles, Paleoceanography, 3(5), 613–619, doi:10.1029/PA003i005p00613, 1988.

QGIS, D. T.: QGIS Geographic Information System, [online] Available from: http://qgis.osgeo.org, 2018.

R Core Team: R: a Language and Environment for Statistical Computing, R Foundation for Statistical computing, Vienna., 2017.

Raddatz, T. J., Reick, C. H., Knorr, W., Kattge, J., Roeckner, E., Schnur, R., Schnitzler, K. G., Wetzel, P. and Jungclaus, J.: Will the tropical land biosphere dominate the climate-carbon cycle feedback during the twenty-first century?, Clim. Dyn., 29(6), 565–574, doi:10.1007/s00382-007-0247-8, 2007.

Ragueneau, O., Tréguer, P., Leynaert, A., Anderson, R. . F., Brzezinski, M. . A., DeMaster, D. . J., Dugdale, R. . C., Dymond, J., Fischer, G., François, R., Heinze, C., Maier-Reimer, E., Martin-Jézéquel, V., Nelson, D. . M. and Quéguiner, B.: A review of the Si cycle in the modern ocean: recent progress and missing gaps in the application of biogenic opal as a paleoproductivity proxy, Glob. Planet. Change, 26(4), 317–365, doi:10.1016/S0921-8181(00)00052-7, 2000.

Rahaman, W., Chatterjee, S., Ejaz, T. and Thamban, M.: Increased influence of ENSO on Antarctic temperature

https://doi.org/10.5194/cp-2020-63
Preprint. Discussion started: 12 May 2020

since the Industrial Era, Sci. Rep., 9(1), 6006, doi:10.1038/s41598-019-42499-x, 2019.

Reynolds, R. W., Rayner, N. A., Smith, T. M., Stokes, D. C., Wang, W., Reynolds, R. W., Rayner, N. A., Smith, T. M., Stokes, D. C. and Wang, W.: An Improved In Situ and Satellite SST Analysis for Climate, J. Clim., 15(13), 1609–1625, doi:10.1175/1520-0442(2002)015<1609:AIISAS>2.0.CO;2, 2002.

Reynolds, R. W., Smith, T. M., Liu, C., Chelton, D. B., Casey, K. S., Schlax, M. G., Reynolds, R. W., Smith, T. M., Liu, C., Chelton, D. B., Casey, K. S. and Schlax, M. G.: Daily High-Resolution-Blended Analyses for Sea Surface Temperature, J. Clim., 20(22), 5473–5496, doi:10.1175/2007JCLI1824.1, 2007.

Riaux-Gobin, C. and Poulin, M.: Possible symbiosis of Berkeleya adeliensis Medlin, Synedropsis fragilis (Manguin) Hasle et al. and Nitzschia lecointei Van Heurck (bacillariophyta) associated with land-fast ice in Adélie Land, Antarctica, Diatom Res., 19(2), 265–274, doi:10.1080/0269249X.2004.9705874, 2004.

Rignot, E., Mouginot, J., Scheuchl, B., van den Broeke, M., van Wessem, M. J. and Morlighem, M.: Four decades of Antarctic Ice Sheet mass balance from 1979–2017, Proc. Natl. Acad. Sci., 116(4), 1095–1103, doi:10.1073/pnas.1812883116, 2019.

Rontani, J.-F., Belt, S. T., Vaultier, F., Brown, T. A. and Massé, G.: Autoxidative and Photooxidative Reactivity of Highly Branched Isoprenoid (HBI) Alkenes, Lipids, 49(5), 481–494, doi:10.1007/s11745-014-3891-x, 2014.

Rontani, J., Smik, L. and Belt, S. T.: Autoxidation of the sea ice biomarker proxy IPSO25 in the near-surface oxic layers of Arctic and Antarctic sediments, Org. Geochem., 129, 63–76, doi:10.1016/J.ORGGEOCHEM.2019.02.002, 2019.

Rontani, J. F., Belt, S. T., Vaultier, F. and Brown, T. A.: Visible light induced photo-oxidation of highly branched isoprenoid (HBI) alkenes: Significant dependence on the number and nature of double bonds, Org. Geochem., 42(7), 812–822, doi:10.1016/j.orggeochem.2011.04.013, 2011.

Rontani, J. F., Charriere, B., Petit, M., Vaultier, F., Heipieper, H. J., Link, H., Chaillou, G. and Sempéré, R.: Degradation state of organic matter in surface sediments from the Southern Beaufort Sea: A lipid approach, Biogeosciences, 9(9), 3513–3530, doi:10.5194/bg-9-3513-2012, 2012.

Sanchez-Cabeza, J.-A., Ruiz-Fernández, A. C., Ontiveros-Cuadras, J. F., Pérez Bernal, L. H. and Olid, C.: Monte Carlo uncertainty calculation of 210Pb chronologies and accumulation rates of sediments and peat bogs, Quat. Geochronol., 23, 80–93, doi:10.1016/J.QUAGEO.2014.06.002, 2014.

Sanchez, N., Reiss, C. S., Holm-Hansen, O., Hewes, C. D., Bizsel, K. C. and Ardelan, M. V: Weddell-Scotia Confluence Effect on the Iron Distribution in Waters Surrounding the South Shetland (Antarctic Peninsula) and South Orkney (Scotia Sea) Islands During the Austral Summer in 2007 and 2008, Front. Mar. Sci., 6(December), 1–16, doi:10.3389/fmars.2019.00771, 2019.

https://doi.org/10.5194/cp-2020-63
Preprint. Discussion started: 12 May 2020


Climate of the Past Discussions

Sangrà, P., Gordo, C., Hernández-Arencibia, M., Marrero-Díaz, A., Rodríguez-Santana, A., Stegner, A., Martínez-Marrero, A., Pelegrí, J. L. and Pichon, T.: The Bransfield current system, Deep Sea Res. Part I Oceanogr. Res. Pap., 58(4), 390–402, doi:10.1016/J.DSR.2011.01.011, 2011.

Sangrà, P., Stegner, A., Hernández-Arencibia, M., Marrero-Díaz, Á., Salinas, C., Aguiar-González, B., Henríquez-Pastene, C. and Mouriño-Carballido, B.: The Bransfield Gravity Current, Deep. Res. Part I Oceanogr. Res. Pap., 119(November 2016), 1–15, doi:10.1016/j.dsr.2016.11.003, 2017.

Schofield, O., Brown, M., Kohut, J., Nardelli, S., Saba, G., Waite, N. and Ducklow, H.: Changes in the upper ocean mixed layer and phytoplankton productivity along the West Antarctic Peninsula, Philos. Trans. R. Soc. A Math. Phys. Eng. Sci., 376(2122), doi:10.1098/rsta.2017.0173, 2018.

Schrader, H. and Gersonde, R.: Diatoms and silicoflagellates, in Micropaleontological Methods and Techniques - An Excercise on an Eight Meter Section of the Lower Pliocene of Capo Rossello, Sicily, Utrecht Micropaleontological Bulletins, vol. 17, edited by W. J. Zachariasse, W. R. Riedel, A. Sanfilippo, R. R. Schmidt, M. J. Brolsma, H. J. Schrader, R. Gersonde, M. M. Drooger, and J. A. Broekman, pp. 129–176., 1978.

Shi, X. and Lohmann, G.: Simulated response of the mid-Holocene Atlantic meridional overturning circulation in ECHAM6-FESOM/MPIOM, J. Geophys. Res. Ocean., 121(8), 6444–6469, doi:10.1002/2015JC011584, 2016.

Shi, X., Lohmann, G., Sidorenko, D. and Yang, H.: Early-Holocene simulations using different forcings and resolutions in AWI-ESM, The Holocene, 095968362090863, doi:10.1177/0959683620908634, 2020.

Sidorenko, D., Goessling, H. F., Koldunov, N. V, Scholz, P., Danilov, S., Barbi, D., Cabos, W., Gurses, O., Harig, S., Hinrichs, C., Juricke, S., Lohmann, G., Losch, M., Mu, L., Rackow, T., Rakowsky, N., Sein, D., Semmler, T., Shi, X., Stepanek, C., Streffing, J., Wang, Q., Wekerle, C., Yang, H. and Jung, T.: Evaluation of FESOM2.0 coupled to ECHAM6.3: Pre-industrial and HighResMIP simulations, J. Adv. Model. Earth Syst., 2019MS001696, doi:10.1029/2019MS001696, 2019.

Simpson, G. L. and Oksanen, J.: Analogue: Analogue Matching and Modern Analogue Technique Transfer Function Models. R Package Version 0.8-2, 2012.

Sinninghe Damsté, J. S. S., Rijpstra, W. I. C. I. C., Coolen, M. J. L. J. L., Schouten, S. and Volkman, J. K. K.: Rapid sulfurisation of highly branched isoprenoid (HBI) alkenes in sulfidic Holocene sediments from Ellis Fjord, Antarctica, Org. Geochem., 38(1), 128–139, doi:10.1016/j.orggeochem.2006.08.003, 2007.

Smik, L., Belt, S. T., Lieser, J. L., Armand, L. K. and Leventer, A.: Distributions of highly branched isoprenoid alkenes and other algal lipids in surface waters from East Antarctica: Further insights for biomarker-based paleo sea-ice reconstruction, Org. Geochem., 95, 71–80, doi:10.1016/J.ORGGEOCHEM.2016.02.011, 2016a.

Smik, L., Cabedo-Sanz, P. and Belt, S. T.: Semi-quantitative estimates of paleo Arctic sea ice concentration based

https://doi.org/10.5194/cp-2020-63
Preprint. Discussion started: 12 May 2020

on source-specific highly branched isoprenoid alkenes: A further development of the PIP 25 index, Org. Geochem., 92, 63–69, doi:10.1016/j.orggeochem.2015.12.007, 2016b.

Stammerjohn, S. E., Martinson, D. G., Smith, R. C. and Iannuzzi, R. A.: Sea ice in the western Antarctic Peninsula region: Spatio-temporal variability from ecological and climate change perspectives, Deep. Res. Part II Top. Stud. Oceanogr., 55(18–19), 2041–2058, doi:10.1016/j.dsr2.2008.04.026, 2008a.

Stammerjohn, S. E., Martinson, D. G., Smith, R. C., Yuan, X. and Rind, D.: Trends in Antarctic annual sea ice retreat and advance and their relation to El Niño–Southern Oscillation and Southern Annular Mode variability, J. Geophys. Res., 113(C3), C03S90, doi:10.1029/2007JC004269, 2008b.

Stastna, V.: Spatio-temporal changes in surface air temperature in the region of the northern Antarctic Peninsula and south Shetland islands during 1950–2003, Polar Sci., 4(1), 18–33, doi:10.1016/j.polar.2010.02.001, 2010.

Stein, R., Fahl, K. and Müller, J.: Proxy Reconstruction of Cenozoic Arctic Ocean Sea-Ice History: from IRD to IP25, Polarforschung, 82(1), 37–71, 2012.

Stevens, B., Giorgetta, M., Esch, M., Mauritsen, T., Crueger, T., Rast, S., Salzmann, M., Schmidt, H., Bader, J., Block, K., Brokopf, R., Fast, I., Kinne, S., Kornblueh, L., Lohmann, U., Pincus, R., Reichler, T. and Roeckner, E.: Atmospheric component of the MPI-M Earth System Model: ECHAM6, J. Adv. Model. Earth Syst., 5(2), 146–172, doi:10.1002/jame.20015, 2013.

Taylor, F., Whitehead, J. and Domack, E.: Holocene paleoclimate change in the Antarctic Peninsula: Evidence from the diatom, sedimentary and geochemical record, Mar. Micropaleontol., 41(1–2), 25–43, doi:10.1016/S0377-8398(00)00049-9, 2001.

Thomas, Allen, Etourneau, King, Severi, Winton, Mueller, Crosta and Peck: Antarctic Sea Ice Proxies from Marine and Ice Core Archives Suitable for Reconstructing Sea Ice over the past 2000 Years, Geosciences, 9(12), 506, doi:10.3390/geosciences9120506, 2019.

Trevena, A. J. and Jones, G. B.: Dimethylsulphide and dimethylsulphoniopropionate in Antarctic sea ice and their release during sea ice melting, Mar. Chem., 98(2–4), 210–222, doi:10.1016/j.marchem.2005.09.005, 2006.

Turner, J., Orr, A., Gudmundsson, G. H., Jenkins, A., Bingham, R. G., Hillenbrand, C.-D. and Bracegirdle, T. J.: Atmosphere-ocean-ice interactions in the Amundsen Sea Embayment, West Antarctica, Rev. Geophys., 55(1), 235–276, doi:10.1002/2016RG000532, 2017.

Turner, J., Marshall, G. J., Clem, K., Colwell, S., Phillips, T. and Lu, H.: Antarctic temperature variability and change from station data, Int. J. Climatol., (June), joc.6378, doi:10.1002/joc.6378, 2019.

Vaughan, D. G., Marshall, G. J., Connolley, W. M., Parkinson, C., Mulvaney, R., Hodgson, D. A., King, J. C., Pudsey, C. J. and Turner, J.: Recent Rapid Regional Climate Warming on the Antarctic Peninsula, Clim. Change,

https://doi.org/10.5194/cp-2020-63
Preprint. Discussion started: 12 May 2020

60(3), 243–274, doi:10.1023/A:1026021217991, 2003.

Vernet, M., Martinson, D., Iannuzzi, R., Stammerjohn, S., Kozlowski, W., Sines, K., Smith, R. and Garibotti, I.: Primary production within the sea-ice zone west of the Antarctic Peninsula: I—Sea ice, summer mixed layer, and irradiance, Deep Sea Res. Part II Top. Stud. Oceanogr., 55(18–19), 2068–2085, doi:10.1016/j.dsr2.2008.05.021, 2008.

Volkman, J. K.: A review of sterol markers for marine and terrigenous organic matter, Org. Geochem., 9(2), 83–99, doi:10.1016/0146-6380(86)90089-6, 1986.

Vorrath, M.-E., Müller, J., Esper, O., Mollenhauer, G., Haas, C., Schefuß, E. and Fahl, K.: Highly branched isoprenoids for Southern Ocean sea ice reconstructions: a pilot study from the Western Antarctic Peninsula, Biogeosciences, 16(15), 2961–2981, doi:10.5194/bg-16-2961-2019, 2019.

Wefer, G., Fischer, G., Füetterer, D. and Gersonde, R.: Seasonal particle flux in the Bransfield Strait, Antartica, Deep Sea Res. Part A. Oceanogr. Res. Pap., 35(6), 891–898, doi:10.1016/0198-0149(88)90066-0, 1988.

Wu, S., Kuhn, G., Diekmann, B., Lembke-Jene, L., Tiedemann, R., Zheng, X., Ehrhardt, S., Arz, H. W. and Lamy, F.: Surface sediment characteristics related to provenance and ocean circulation in the Drake Passage sector of the Southern Ocean, Deep Sea Res. Part I Oceanogr. Res. Pap., 154, 103135, doi:10.1016/j.dsr.2019.103135, 2019.

Xiao, X., Fahl, K. and Stein, R.: Biomarker distributions in surface sediments from the Kara and Laptev seas (Arctic Ocean): indicators for organic-carbon sources and sea-ice coverage, Quat. Sci. Rev., 79, 40–52, doi:10.1016/j.quascirev.2012.11.028, 2013.

Yuan, X.: ENSO-related impacts on Antarctic sea ice: a synthesis of phenomenon and mechanisms, Antarct. Sci., 16(4), 415–425, doi:10.1017/S0954102004002238, 2004.

Zhou, M., Niiler, P. P. and Hu, J. H.: Surface currents in the Bransfield and Gerlache Straits, Antarctica, Deep. Res. Part I Oceanogr. Res. Pap., 49(2), 267–280, doi:10.1016/S0967-0637(01)00062-0, 2002.

Zwally, H. J., Comiso, J. C., Parkinson, C. L., Cavalieri, D. J. and Gloersen, P.: Variability of Antarctic sea ice 1979–1998, J. Geophys. Res., 107(C5), 3041, doi:10.1029/2000JC000733, 2002.

https://doi.org/10.5194/cp-2020-63
Preprint. Discussion started: 12 May 2020

Climate of the Past Discussions
Open Access
EGU

Figures

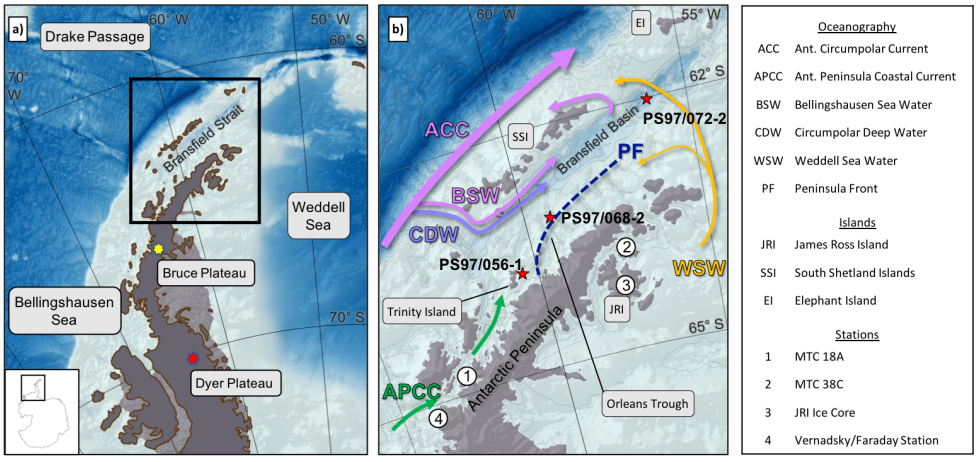

Figure 1: a) Overview map of the Antarctic Peninsula with the position of the Dyer Plateau (Abram et al., 2010),(Abram et al., 2010)(Abram et al., 2010)(Abram et al., 2010)(Abram et al., 2010)(Abram et al., 2010) Bruce Plateau (Goodwin et al., 2016) and bathymetric features in the Bellingshausen Sea, the Weddell Sea and the Drake Passage. B) Oceanographic setting in the study area (modified after Hofmann et al., 1996; Moffat and Meredith, 2018; Sangrà et al., 2011), sediment and ice core locations and geographic locations mentioned in the text. Maps were generated with QGIS 3.0 (2018) and the bathymetry was taken from GEBCO_14 from 2015.

https://doi.org/10.5194/cp-2020-63
Preprint. Discussion started: 12 May 2020

Climate of the Past
Discussions
Open Access
EGU

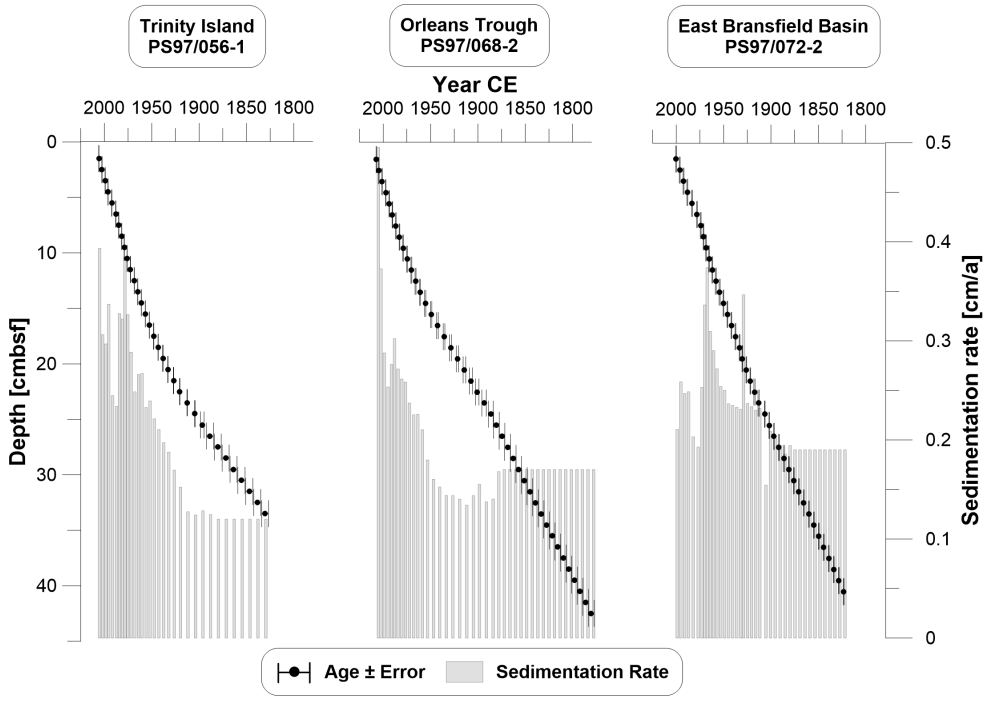

Figure 2: Age-depth models with error bars of all three core sites. The sedimentation rate is displayed in grey bars. Ages were extrapolated prior to 1880 CE for all cores based on their average respective sedimentation rate for the oldest 3 cm. All plots were done with Grapher™ 13.

1090

https://doi.org/10.5194/cp-2020-63
Preprint. Discussion started: 12 May 2020

Climate of the Past Discussions
Open Access
EGU

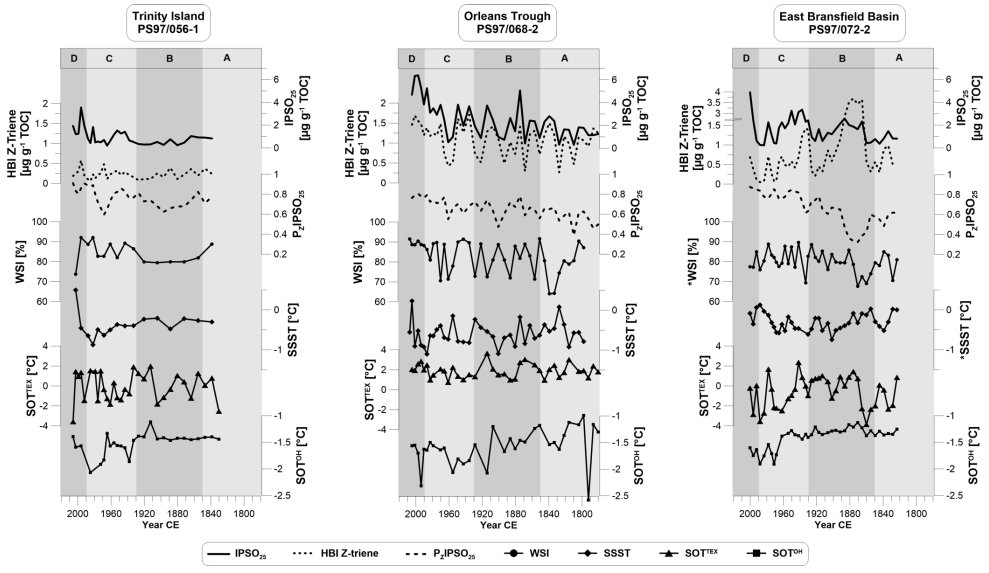

Figure 3: Biomarker composition of the three sediment cores showing concentrations of (from top to bottom) $IPSO_{25}$ and HBI Z-trienes, the sea ice index P_ZIPSO_{25}, diatom-derived winter sea ice (WSI) concentrations and temperatures of summer sea surface temperatures (SSST), subsurface ocean temperature derived from TEX^L_{86} (SOT^{TEX}), and OH-GDGTs (SOT^{OH}). Data marked with * are from the trigger core PS97/072-1. Vertical grey bars denote the stratigraphic units A to D.

https://doi.org/10.5194/cp-2020-63
Preprint. Discussion started: 12 May 2020

Climate of the Past Discussions
Open Access
EGU

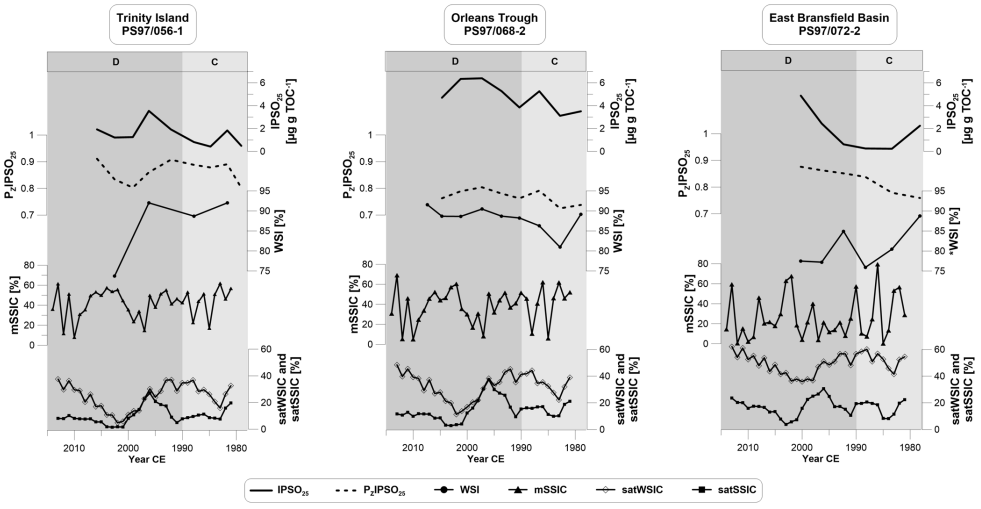

Figure 4: Concentrations of (from top to bottom) $IPSO_{25}$, P_ZIPSO_{25}, WSI compared to modelled spring sea ice concentrations (mSSIC) and satellite derived winter and spring sea ice concentrations (satWSIC and satSSIC, 5 year running mean) from the National Snow and Ice Data Center (NSIDC, Cavalieri et al., 1996) for all three core sites. Data marked with * are from the trigger core PS97/072-1. Vertical grey bars denote the stratigraphic units C and D.

https://doi.org/10.5194/cp-2020-63
Preprint. Discussion started: 12 May 2020

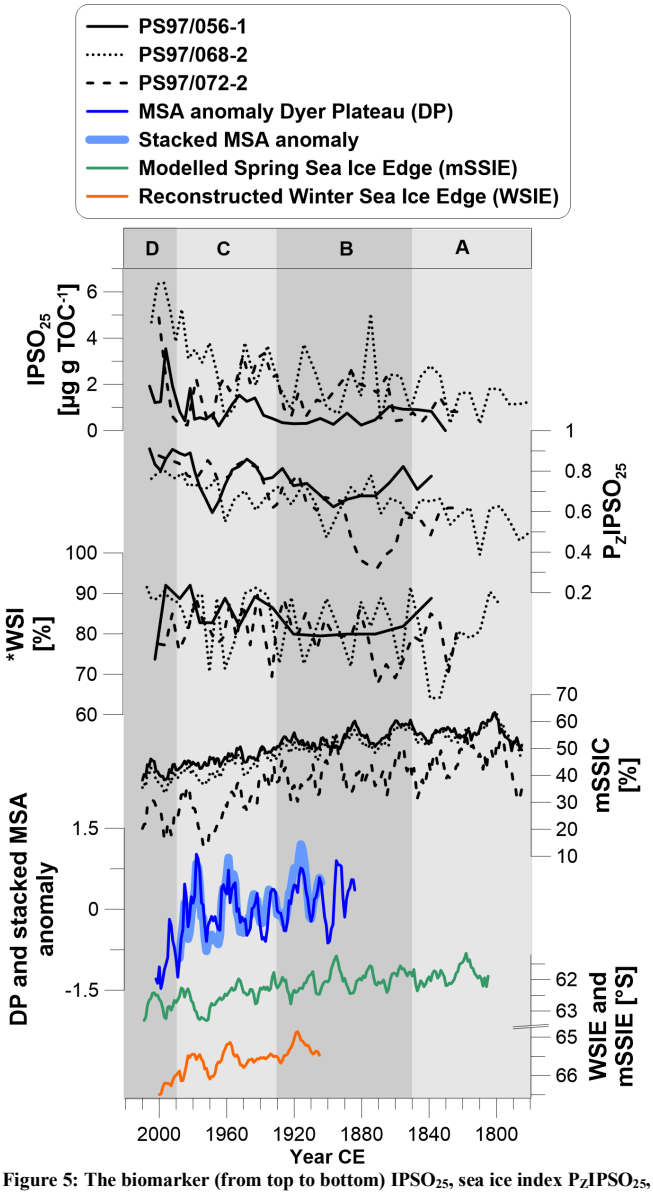

Figure 5: The biomarker (from top to bottom) $IPSO_{25}$, sea ice index P_ZIPSO_{25}, and winter sea ice concentration (WSI) from diatom assemblages compared to modelled spring sea ice cover (mSSIC, 10 year running mean), MSA anomaly from Dyer Plateau and stacked MSA covering the Bellingshausen Sea sector (5 year running mean, Abram et al., 2010), modelled spring sea ice edge latitude (mSSIE, 10 year running mean) and econstructed winter sea ice edge latitude from MSA (WSIE, 10 year running mean, Abram et al., 2010). Data marked with * are from the trigger core PS97/072-1. Vertical grey bars denote the stratigraphic units A to D.

https://doi.org/10.5194/cp-2020-63
Preprint. Discussion started: 12 May 2020

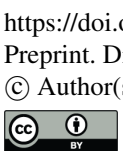

Climate of the Past
Discussions
Open Access
EGU

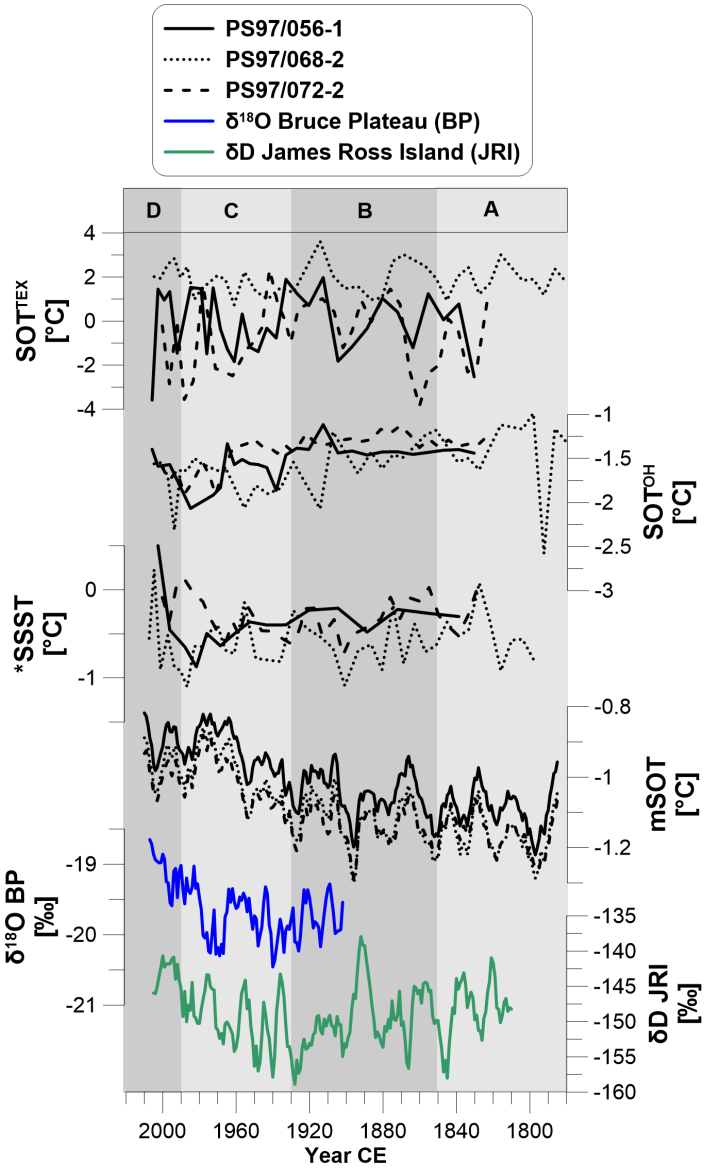

Figure 6: Biomarker derived subsurface ocean temperatures based on TEX^{L}_{86} (SOT^{TEX}), and hydroxylated GDGTs (SOT^{OH}), and summer sea surface temperatures (SSST) derived from diatom assemblages compared to modelled subsurface ocean temperature (mSOT), stable isotope ice core records from the Bruce Plateau (BP, $\delta^{18}O$, 5 year running mean; Goodwin et al., 2016) and from James Ross Island (JRI, δD, 5 year running mean; Abram et al., 2013). Data marked with * are from the trigger core PS97/072-1. Vertical grey bars denote the stratigraphic units A to D.

https://doi.org/10.5194/cp-2020-63
Preprint. Discussion started: 12 May 2020

Climate of the Past Discussions
Open Access
EGU

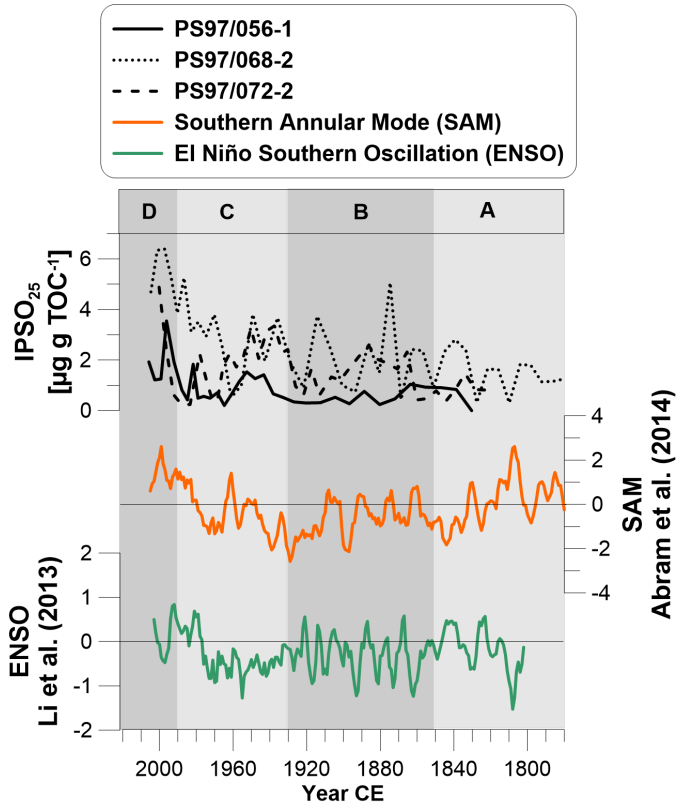

Figure 7: Concentrations of biomarker $IPSO_{25}$ in all three sediment cores compared to circulation pattern of the Southern Annular Mode (SAM, 5 year running mean; Abram et al., 2014), and the El Niño Southern Oscillation (ENSO, 5 year running mean; Li et al., 2013). Vertical grey bars denote the stratigraphic units A to D.